Circuits and Systems
Mekelweg 4,
2628 CD Delft
The Netherlands
http://ens.ewi.tudelft.nl/



M.Sc. Thesis

Transmitter measurements and analysis of frame synchronisation of an Impulse-Radio Ultra-wideband System

Ananthakrishnan Ramkumar
4119568



Transmitter measurements and analysis of frame synchronisation of an Impulse-Radio Ultra-wideband System

Thesis

submitted in partial fulfillment of the
requirements for the degree of

Master of Science

in

Electrical Engineering

by

Ananthakrishnan Ramkumar
born in Salem, India

This work was performed in:

Wireless Group
Holst Centre/imec
High Tech Campus 31
5656 AE, Eindhoven, the Netherlands



Delft University of Technology

Copyright © 2012 Circuits and Systems Group
All rights reserved.

Delft University of Technology
Department of
Telecommunications

The undersigned hereby certify that they have read and recommend to the Faculty of Electrical Engineering, Mathematics and Computer Science for acceptance a thesis entitled **"Transmitter measurements and analysis of frame synchronisation of an Impulse-Radio Ultra-wideband System"** by **Ananthakrishnan Ramkumar** in partial fulfillment of the requirements for the degree of **Master of Science**.

Dated: 21 Aug 2012

Advisors:

Dr.ir.Gerard Janssen

ing.Hans Pflug (Holst Centre/imec)

Committee Members:

Dr.ir.Jos Weber

Abstract

Ultra-wideband (UWB) is a promising radio technology which is well suited to low power short-range wireless applications. At Holst Centre, there is a research program on the design and implementation of ultra low power, Impulse Radio-UWB (IR-UWB) wireless systems suitable for audio streaming and real time localization systems. Some key technology challenges for IR-UWB systems are Direct Current (DC) power consumption, Link-budget and Quality of Service (QoS).

The first part of this thesis focuses on measurement of DC power consumption, transmit output power and spectrum using the IR-UWB transmitter. As the hardware supports several modes, an automated measurement setup with programmable parameters has been created. In the second part, a mathematical model for the preamble and Start of Frame Delimiter (SFD) detection stages of the receiver operation is provided. This part of the receiver is a critical one and is challenging for IR-UWB type of signals due to the low transmit power. A method to estimate the signal to noise ratio (SNR) per pulse from the output of the preamble detection block is proposed. A theoretical approach for setting the threshold for SFD detection is described. It is shown through simulations that this method of threshold setting provides a significant improvement in receiver performance.

Acknowledgments

I would like to thank my supervisor Hans Pflug for giving me the opportunity to do my master thesis work at Holst Centre/imec. I would like to thank him for his constant guidance and encouragement throughout the duration of my thesis. Thanks for being a pleasant supervisor to work with.

I would like to thank my advisor Dr.ir.Gerard Janssen for his timely guidance, support and motivation. I thank him for reviewing my work critically and providing valuable feedback and comments.

I would like to thank Alex, Jac, Johan and Xiaoyan for their interest in my work and for providing valuable technical inputs. I have learnt a lot from our interactions. I would also like to express my gratitude to all the employees of imec for providing a friendly atmosphere to work in.

I would like to thank committee member Dr.ir.Jos Weber for his time and interest to review this work.

I thank my friends in Delft and IMEC for their encouragement and for making my stay in the country enjoyable.

Last but not least, I would like to thank my family for their constant motivation, support and love. Without them this would not have been possible.

Ananthakrishnan Ramkumar
Delft, The Netherlands
21 Aug 2012

Contents

Abstract v

Acknowledgments vii

Abbreviations xv

Notation xvii

1 Introduction 1
- 1.1 Motivation . . . 1
- 1.2 Outline . . . 3

2 Background 5
- 2.1 Frame structure . . . 5
  - 2.1.1 SHR preamble . . . 5
  - 2.1.2 PHR and PSDU Symbol structure . . . 6
  - 2.1.3 Scrambler . . . 7
  - 2.1.4 Pulse repetition frequency . . . 7
- 2.2 System overview . . . 8
  - 2.2.1 Transmitter . . . 9
  - 2.2.2 Receiver . . . 9
  - 2.2.3 Types of detection . . . 11

3 Transmitter measurements 13
- 3.1 Description of Setup . . . 13
- 3.2 Transmit spectrum . . . 15
  - 3.2.1 Automation of Measurements using MATLAB . . . 15
  - 3.2.2 Average Power . . . 15
  - 3.2.3 Peak Power . . . 19
- 3.3 Pulse shape . . . 21
- 3.4 DC Power consumption . . . 21
- 3.5 Summary . . . 24

4 Preamble detection 25
- 4.1 Introduction . . . 25
- 4.2 Coherent case . . . 27
  - 4.2.1 Distribution of Max . . . 28
  - 4.2.2 Estimating SNR in the coherent case . . . 29
  - 4.2.3 Number of frames required: an example . . . 31
- 4.3 Non-coherent case . . . 31
  - 4.3.1 Estimating the SNR in non-coherent case . . . 33
  - 4.3.2 Number of frames required: an example . . . 34

4.4 Summary 35

5 SFD Detection Analysis **37**
5.1 Introduction 37
5.1.1 Current implementation 37
5.2 System model 38
5.3 Coherent case 39
5.3.1 Symbol correlation 39
5.3.2 SFD correlation 40
5.3.3 Evaluation of threshold 43
5.4 Non-coherent case 46
5.4.1 Symbol Correlation 46
5.4.2 SFD correlation 48
5.4.3 Evaluation of Threshold 52
5.5 Results 54
5.6 Summary 56

6 Conclusions **57**
6.1 Main contributions and results 57
6.2 Directions for future work 58

A Appendix A **61**
A.1 Standard modes 61
A.2 Calculating IR-UWB Signal Power 61
A.2.1 Average and Peak Signal Power 61
A.2.2 Regulatory Signal Power 62
A.3 Probability distributions 63

List of Figures

1.1 Applications of UWB 2

2.1 UWB frame format (source: IEEE 802.15.4a standard) 5
2.2 Format of SHR preamble 6
2.3 UWB PHY Symbol structure 7
2.4 Summary of frame structure 8
2.5 Transceiver block diagram (source: Holst Centre/imec) 9
2.6 Transmitter block diagram (source: Holst Centre/imec) 10
2.7 Coherent receiver architecture (source: Holst Centre/imec) 10
2.8 ASIC block (source: Holst Centre/imec) 11
2.9 IEEE 802.15.4a Frame structure 11
2.10 IR-UWB receiver developed by Holst Centre/imec 12

3.1 TX measurement setup 13
3.2 TX block diagram 14
3.3 Transmitter spectrum measurement 15
3.4 Average power spectrum measured in 1 MHz, 1 ms sweep time per point. The red line indicates the -10 dB bandwidth 16
3.5 Frame-level dutycycling 16
3.6 Average power measurement spectrum, measured in 1 MHz with sweep time 2ms per point in mode 1.2. The red line shows the -10 dB bandwidth 17
3.7 Transmitter output spectrum with IEEE 802.15.4a spectrum mask . . . 18
3.8 Measured burst using scrambling code with phase-inversions (captured on LeCroy serial data analyzer, 40 GS/s) 18
3.9 Measured burst using zero-phase-inversion scrambling code (captured on LeCroy serial data analyzer, 40GS/s) 20
3.10 Measured peak power spectrum (dBm) in 8 MHz of a complete frame consisting of bursts having no phase changes. For this measurement a spectrum analyzer is used (frequency domain measurement) 21
3.11 Exponential pulse (captured using Lecroy oscilloscope) 22
3.12 RC pulse-shaping circuit in TX 22
3.13 Relative PSD with varying register settings for bias current and load capacitance 23

4.1 Preamble correlation block (source: Holst Centre/imec) 26
4.2 List of all the length 31 preamble codes in the standard 26
4.3 Preamble correlation for L=2 accumulations, no noise 28
4.4 Preamble correlation for L=2 accumulations, adding noise 28
4.5 Noise estimate in coherent case (statistics using 100 values) 30
4.6 Amplitude estimate in coherent case (statistics using 100 values) 30
4.7 Noise estimate in coherent case (statistics using 1000 values) 30
4.8 Amplitude estimate in coherent case (statistics using 1000 values) . . . 30
4.9 SNR estimate in coherent case (statistics using 100 values) 31

4.10 SNR estimate in coherent case (statistics using 1000 values) 31
4.11 Non-coherent preamble correlation for L=2 accumulations using unsigned coefficients, no noise 32
4.12 Non-coherent preamble correlation for L=2 accumulations using unsigned coefficients, adding noise 32
4.13 Non-coherent preamble correlation for L=2 accumulations using signed coefficients, no noise 33
4.14 Non-coherent preamble correlation for L=2 accumulations using signed coefficients, adding noise 33
4.15 Noise estimate in non-coherent case (statistics using 1000 monte-carlo runs) 33
4.16 Amplitude estimate in non-coherent case (statistics using 1000 monte-carlo runs) 33
4.17 SNR estimate in non-coherent case (statistics using 1000 monte-carlo runs) 34

5.1 SFD detection block diagram 37
5.2 SFD correlation output with noise 38
5.3 SHR preamble 39
5.4 SHR preamble symbols without adding noise; (*above*) before symbol correlation and (*below*) after symbol correlation 40
5.5 SFD correlation output (y) in coherent case 41
5.6 Cross-correlation of SHR preamble with the SFD sequence (without adding noise) 41
5.7 PDFs of SFD peak and maximum of side-peaks during coherent detection at -15 dB received SNR per pulse, amplitude A=1 45
5.8 Sweeping through threshold (γ) to choose optimal threshold that maximizes P_d at -15 dB SNR per pulse, amplitude A=1 46
5.9 Correlation of absolute value of preamble symbols with absolute value of SFD 48
5.10 SFD correlation of SHR preamble with *SFDm* in non-coherent case . . 49
5.11 SFD correlation output (y) in non-coherent case 49
5.12 PDFs of SFD peak and maximum of side-peaks during non-coherent detection at -3 dB received SNR per pulse, amplitude A=1 53
5.13 Sweeping through threshold (γ) to choose optimal threshold that maximizes P_d at -3 dB SNR per pulse, taking A=1 54
5.14 SFD detection threshold vs SNR in Coherent case, for amplitude A=1 . 55
5.15 SFD detection threshold vs SNR in Non-coherent case, for amplitude A=1 55
5.16 SFD detection probability curves: Coherent and Non-coherent 55

A.1 fig:IEEE 802.15.4a IR-UWB signal example showing V_{pk} being the peak amplitude. 62

List of Tables

2.1 IEEE 802.15.4a UWB pulse durations 9

3.1 DC current measurement: duty cycled mode, divider switched off . . . 23
3.2 DC current measurement: continuous mode, divider switched off 23

A.1 Standard modes 61
A.2 Mode dependent parameter values 62
A.3 Summary 63

Abbreviations

ADC	Analog to Digital Converter
AGC	Automatic Gain Control
ASIC	Application Specific Integrated Circuit
AWGN	Additive White Gaussian Noise
BPM	Burst Position Modulation
BPSK	Binary Phase Shift Keying
CDF	Cumulative Distribution Function
CIR	Channel Impulse Response
CLT	Central Limit Theorem
CML	Current Mode Logic
DBB	Digital Baseband
DAC	Digital to Analog Converter
DCO	Digitally Controlled Oscillator
DSP	Digital Signal Processor
FCC	Federal Communications Commission
FE	Front End
FEC	Forward Error Correction
FO	Frequency Offset
FPGA	Field-Programmable Gate Array
GPIB	General Purpose Interface Bus
I^2S	Inter-IC Sound
I.I.D	Independent and Identically Distributed
IEEE	Institute of Electrical and Electronics Engineers
I	In-phase
IR-UWB	Impulse Radio Ultra-Wideband
LFSR	Linear Feedback Shift Register
LNA	Low Noise Amplifier
PDF	Probability Density Function
PHR	PHY Header
PHY	Physical layer
PLL	Phase Locked Loop
PPM	Parts Per Million
PSD	Power Spectral Density
PSDU	PHY Protocol Data Unit
PSDU	PHY Service Data Unit
PRF	Pulse Repetition Frequency
Q	Quadrature phase
RBW	Resolution Bandwidth
RC	Resistor-Capacitor
RF	Radio Frequency
RMS	Root Mean Square
RX	Receiver

SAA	Small Amplitude Approximation
SFD	Start of Frame Delimiter
SHR	Synchronisation Header
SNR	Signal to Noise Ratio
SPI	Serial Peripheral Interface
TSPC	True Single Phase Clocked
TX	Transmitter
UWB	Ultra-wideband
VBW	Video Bandwidth
VGA	Variable Gain Amplifier
WSN	Wireless Sensor Network

Notation

A	Amplitude of UWB pulse
C_i	Preamble code sequence
L	Number of accumulations in preamble detection block
Len	Length of array
Max	Maximum of preamble correlation outputs for all chip positions
Min	Minimum of preamble correlation outputs for all chip positions
N	Number of chip positions per preamble symbol
N_{burst}	Number of burst positions per symbol period
N_{cpp}	Number of chips per pulse
N_{hop}	Number of hop positions per symbol
N_{cpb}	Number of chips per burst
N_c	Number of chip durations per symbol
N_{cps}	Number of chips per symbol
N_{cg}	Number of chips per guard interval
N_{SFD}	Number of SFD symbols
N_{SYNC}	Number of SYNC symbols
$SFDm$	Modified SFD sequence for non-coherent detection
μ_{rice}	Rician mean of magnitude of received chips
$\mu_{rayleigh}$	Rayleigh mean of magnitude of received chips
S_i	Preamble symbol
σ_c	Complex noise variance
σ	Noise variance in either of I (or Q) component
σ_{rice}	Rician distribution parameter of magnitude of received chips
$\sigma_{rayleigh}$	Rayleigh distribution parameter of magnitude of received chips
$\tau_{b,eff}$	Effective burst width
T_{burst}	Time duration of a PSDU burst
T_c	Chip duration
T_p	Pulse duration
T_{sym}	PSDU Symbol duration
τ	Time constant of exponential pulse shape
Z_o	Characteristic impedance of antenna

1 Introduction

The increasing popularity of portable electronic devices has given rise to the need for short range wireless links which provide communication capability without the need for cables. Since these devices are battery driven, low power consumption is key. Ultra-wideband (UWB) radio technology has many attributes that make it an attractive communication method for battery operated and even battery-less devices [1].

Ultra-wideband(UWB) radio technology uses very large bandwidth and low transmit power for short to medium range communication. UWB signals are defined by the Federal Communications Commission (FCC) as having emission bandwidths exceeding the lesser of 500 MHz or 20% of the arithmetic center frequency. Transmitted power density is limited to be less than -41.3 dBm/MHz in the 3.1-10.6 GHz band [2].

Although UWB communication started to gain much interest in the industry only a few years ago, it has its origin in the early days of wireless transmission. In 1893 Heinrich Hertz performed experiments using a spark discharge to generate frequencies in the range of 50-500 MHz and such spark gaps and arc discharges can be seen as the first impulse radio systems [3]. Modern impulse radio UWB (IR-UWB) systems use simple electronics circuits to generate narrow pulses in time for transmission.

Due to the large bandwidth, UWB signals are robust to fading and allow fine time resolution. Since the center frequency is relatively low, UWB signals can penetrate many materials and hence can be used in indoor environments as well. Another important aspect is the very low transmit power causing low level of interference to other existing wireless systems in the same frequency range. Use of narrow pulses allows duty-cycling of the radio which results in low power consumption. These properties make UWB suitable for low power short-to-medium range communication and localization systems. Applications that have been considered include wireless sensor networks (WSNs), sensing and positioning systems, inter-chip communication, contact-less wireless biological or biomedical networks and imaging systems [4].

1.1 Motivation

At Holst Centre, there is a research program on the design and implementation of ultra low power, IR-UWB wireless systems suitable for audio streaming and real time localization systems. The IR-UWB system is based on the IEEE 802.15.4a standard [5]. The standard supports several modes of operation by providing flexible physical layer parameters. Some key technology challenges for IR-UWB systems are DC power consumption, Link budget and Quality of Service (QoS).

As IR-UWB systems are targeted at battery operated devices, low power consumption is an important requirement. Power consumption can be lowered by duty-cycling the transceiver. This is possible in IR-UWB systems since the pulses are not present



Figure 1.1: Applications of UWB

all the time. The DC consumption depends on the duty-cycling ratio which in turn depends on the physical layer parameters of the operating mode. Measurement of the power consumption is therefore required to evaluate the gain provided by duty-cycling for different modes.

The link budget of the system gives an indication of the communication range. The link budget depends on the transmit output power and receiver sensitivity. The 802.15.4a standard specifies limits on the transmit power and requirements on the emission bandwidth for UWB signals. Hence, measurements of the transmit output power and spectrum are required to check compliance with the standard. In order to get the link budget, measurement of the receiver sensitivity for different modes of operation is required.

The first part of the thesis work, therefore, focused on the system analysis and measurement of DC power consumption, receiver sensitivity and transmitter output power and spectrum for different modes of operation. An automated measurement setup with programmable settings for measuring transmitter output power and spectrum has been created. By changing the parameters, measurements can be performed for various modes. The measurement results for one of the supported modes is presented in the report. The measurement of receiver sensitivity, however, could not be done due to problems with the receiver.

Preamble detection and Start of Frame Delimiter (SFD) detection are two important operations performed by the baseband receiver of the IR-UWB system. The decoding of

payload can start only after this. Preamble detection is required to detect the presence of signal and synchronize to the start of the symbols. This is followed by SFD detection which informs the receiver of the start of the payload. A detection threshold is used for this purpose. So far the setting of detection thresholds was done in a fairly simple way, based on statistics computed by collecting large number of frames. This method of threshold setting is not very efficient as large number of frames may be wasted before a suitable threshold is set. Therefore, theoretical method to determine the optimal threshold for SFD detection is needed.

Consequently, the analysis of the receiver preamble and SFD detection was done. A theoretical approach for setting the threshold level has been described. The optimal threshold depends on the received pulse amplitude and noise variance. A method to estimate the pulse amplitude, noise variance and hence the signal to noise ratio in the preamble detection stage is proposed. The detection performance of the analytical threshold is verified using simulations.

As the receiver was not functioning properly till the end of the project, the implications of the theoretical work could not be verified with measurements unfortunately, although some first implementations show promising results.

1.2 Outline

The thesis report is organized as follows:

Chapter 2: Background

This chapter provides an overview of the PHY specifications of the IEEE 802.15.4a standard. Next a brief description of the transceiver is provided including both the analog and digital blocks. The operation of the digital baseband receiver is explained.

Chapter 3: Transmitter measurements

This chapter provides the results of measurements performed using the IR-UWB transmitter board. The programmable setup used to automate the measurements is described. The peak and average TX output power measurements are reported and compliance of the TX output to the spectral mask is verified. Next, the effect of changing the pulse shape on the output spectrum is analyzed. Finally a comparison of DC power consumption in the continuous and duty-cycled cases is given.

Chapter 4: Preamble detection

In this chapter, firstly the method used for detection of the Synchronisation Header (SHR) preamble is explained. Expressions for the probability distributions of the outputs of the preamble detection block is presented for both coherent and non-coherent cases. A method to estimate the signal-to-noise ratio (SNR) per pulse using the outputs of the preamble detection block is proposed.

Chapter 5: SFD detection

In this chapter, detection of the Start of Frame Delimiter (SFD), which marks the start of the payload, is described. A mathematical approach to determine the optimal detection threshold is derived for coherent and non-coherent cases. The detection performance using the analytical threshold is compared to the current implementation.

Chapter 6: Conclusions

The main results of this thesis are summarized and directions for future work are highlighted in this chapter.

Background 2

Low power consumption is one of the main targets in designing a radio for a Wireless Sensor Network (WSN) with power scavenging as the ultimate goal. Impulse radio ultra-wideband (IR-UWB) has properties that make it a viable solution for the type of applications and environments used with WSNs [6]. The low average power consumption of these systems is attributed to the low duty-cycle of IR-UWB pulses which allows the radio front end to be switched off between pulse transmissions/receptions.

The IR-UWB system is developed based on the IEEE 802.15.4a standard. This chapter provides an overview of the PHY specifications of the 802.15.4a standard. This is followed by a brief description of the low power architecture of the IR-UWB system.

2.1 Frame structure

The 802.15.4a standard provides several modes of operation for the UWB radio (see Appendix A.1 for a list of modes). The UWB PHY waveform is based upon an impulse radio signalling scheme using band-limited data pulses. The standard specifies channels in the frequency range of 3-10 GHz.

The UWB frame format prescribed in the standard IEEE 802.15.4a consists of a Synchronisation Header (SHR) preamble first, followed by the PHY header (PHR) and finally the PHY service data unit (PSDU).

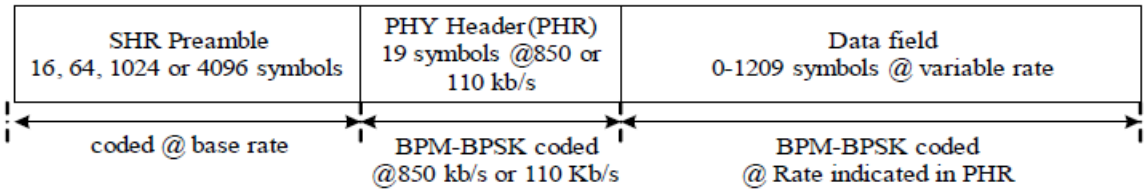

Figure 2.1: UWB frame format (source: IEEE 802.15.4a standard)

The SHR consists of a given sequence of isolated pulses. It allows the receiver to perform timing acquisition. The purpose of the PHR is to inform the RX about the structure of the PSDU. It consists of 19 bits including preamble duration, nominal data rate, frame length, ranging bit and parity bits (Hamming code). The PSDU contains bytes of payload.

2.1.1 SHR preamble

The SHR preamble is added prior to the PHR to aid receiver algorithms related to AGC setting, antenna diversity selection, timing acquisition, coarse and fine frequency

recovery, packet and frame synchronisation, channel estimation, and leading edge signal tracking for ranging [5]. The format of the SHR preamble is given in Figure 2.2. It consists of two portions: SYNC which consists of 16/64/1024/4096 symbols and the SFD which consists of 8/64 symbols. The number of SYNC symbols can be chosen depending on the signal-to-noise ratio (SNR), usage type etc. and is independent of the mode. The choice of SFD symbols depends on the mode. The SYNC portion is required for packet synchronization, channel estimation and ranging. SFD detection is important to establish frame timing.

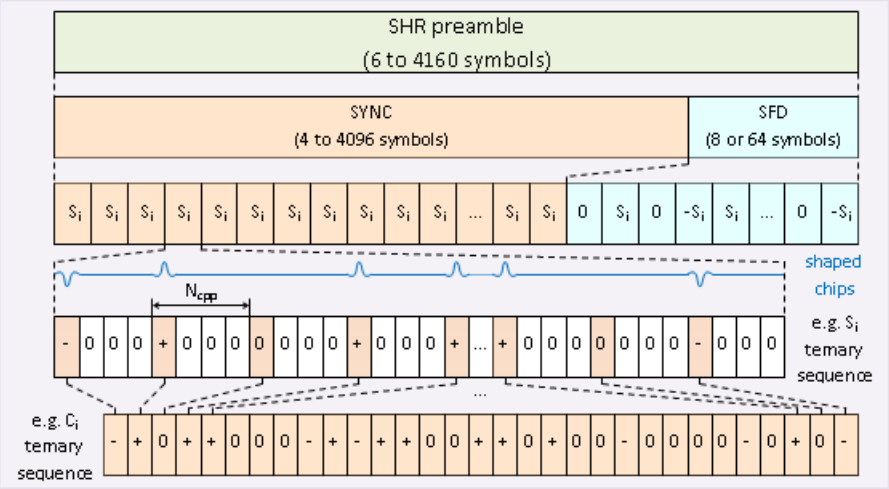

Figure 2.2: Format of SHR preamble

A preamble code C_i is used to construct symbols that constitute the SYNC portion of the SHR preamble. The SHR SYNC field is constructed by repetition of the preamble symbol S_i, where S_i is the preamble code sequence C_i spread by $\delta_{N_{cpp}}$ of length N_{cpp}, which consists of a 1 followed by $(N_{cpp} - 1)$ zeros.

The UWB PHY supports two lengths of preamble: a length 31 code and an optional length 127 code. The preamble code is a sequence of code symbols drawn from a ternary alphabet (-1,0,1) and selected for use in the UWB PHY because of their perfect autocorrelation properties. A UWB pulse with the corresponding polarity is transmitted for every non-zero code position of the preamble.

2.1.2 PHR and PSDU Symbol structure

A combination of burst pulse position modulation (BPM) and binary phase-shift keying (BPSK) is used to support both coherent and noncoherent receivers using a common signaling scheme. The combined BPM-BPSK is used to modulate the symbols, with each symbol being composed of an active burst of UWB pulses.

Each symbol consists of an integer number of possible chip positions, N_c, each with duration T_c. The overall symbol duration denoted by T_{sym} is given by $T_{sym} = N_c T_c$. Furthermore, each symbol is divided into two equal BPM intervals of duration $T_{BPM} = T_{sym}/2$. A burst is formed by grouping N_{cpb} consecutive chips and has duration $T_{burst} = N_{cpb} T_c$ as shown in Figure 2.3. The location of the burst in either the first half

or second half of the symbol indicates one bit of information. Additionally the phase of the burst (either 0 or π) is used to indicate a second bit of information.

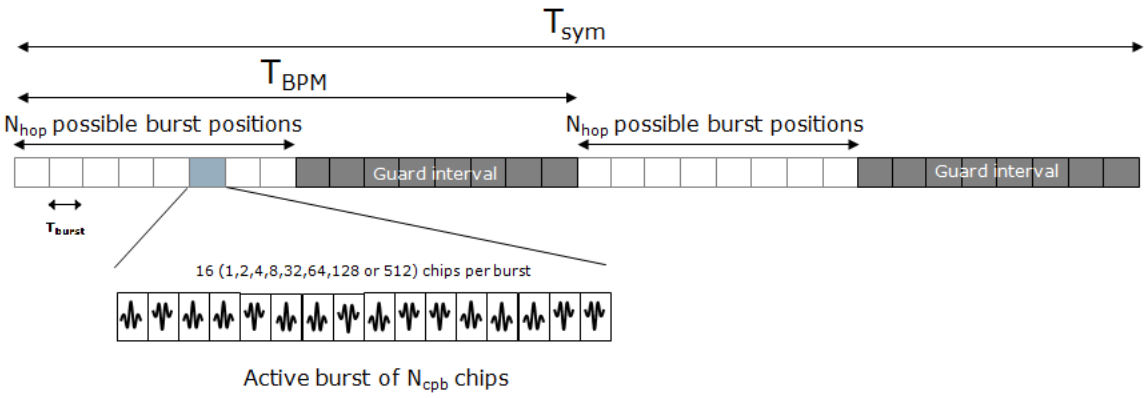

Figure 2.3: UWB PHY Symbol structure

In each UWB PHY symbol interval, a single burst is transmitted. The fact that burst duration is typically much shorter than the BPM duration, i.e. $T_{burst} \ll T_{BPM}$, provides for some multi-user access interference rejection in the form of time hopping. The total number of burst durations per symbol, N_{burst}, is given by $N_{burst} = T_{sym}/T_{burst}$. The duty-cycling ratio (dc) is related to the number of bursts per symbol as

$$dc = \frac{1}{N_{burst}} \tag{2.1}$$

In order to limit the amount of inter symbol interference caused by multipath, only the first half of each T_{BPM} period shall contain a burst. Therefore only the first $N_{hop} = N_{burst}/4$ possible burst positions are candidate hopping burst positions within each BPM interval. Each burst position can be varied on a symbol-to-symbol basis according to a time hopping code generated by a scrambler.

2.1.3 Scrambler

The UWB PHY uses a scrambler spreader for modulation of symbols and for generating the hopping code. The burst hopping provides for multi-user interference rejection. The chip scrambling sequence provides additional interference suppression among coherent receivers as well as spectral smoothing of the transmitted waveform.

The scrambler is realized using linear feedback shift registers (LFSR). The LFSR is initialized upon the transmission of bit 0 of the PHR. The initial state of the LFSR is determined from the preamble code.

2.1.4 Pulse repetition frequency

The mean pulse repetition frequency (PRF) is defined as the total number of pulses emitted during a symbol period divided by the length of the symbol duration. The peak PRF corresponds to the highest frequency at which a standard compliant transmitter

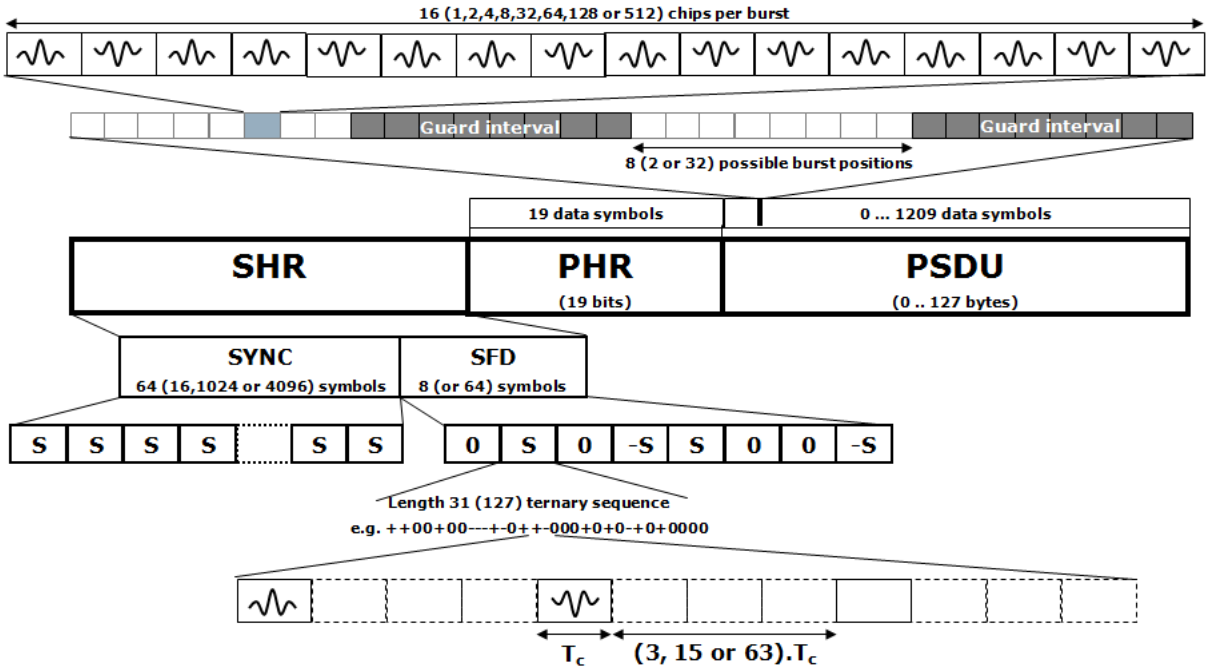

Figure 2.4: Summary of frame structure

shall emit pulses. During the data portion of a PPDU, the peak and mean PRFs differ due to grouping of pulses into bursts (consecutive chip durations). The peak PRF is related inversely to the chip duration (eg. 499.2 MHz for 2 ns chip duration). The mean PRF for the PSDU is given by, $PRF = 1/T_{sym}$. During the SHR preamble portion of the UWB frame, however, the peak is lower since pulses are emitted uniformly at an interval of N_{cpp} chip durations during each preamble symbol. The peak PRF, $pPRF$ for the SHR is given by $pPRF = 1/(T_c\, N_{cpp})$ and the mean PRF is given by $mPRF = pPRF * (16/31)$ or $pPRF * (64/127)$, with 16, 64 representing the number of non-zero values in the length 31 and length 127 C_i codes respectively.

2.2 System overview

The system diagram of the UWB transceiver is shown in Figure 2.5.

In the sensor/transducer domain an analog signal is acquired and/or produced. For e.g. audio signal received from a microphone or data sent to an earpiece. The data is exchanged with the receiver baseband using serial peripheral interface (SPI) (asynchronous) and/or I^2S (synchronous) interface. The transceiver also includes the receiver analog front-end and transmitter (digital baseband and analog front-end integrated). The analog front end provides all clocks for the receiver and includes the low noise amplifier (LNA), mixer and variable gain amplifier (VGA). The TX and RX analog front-end are controlled by a SPI bus.

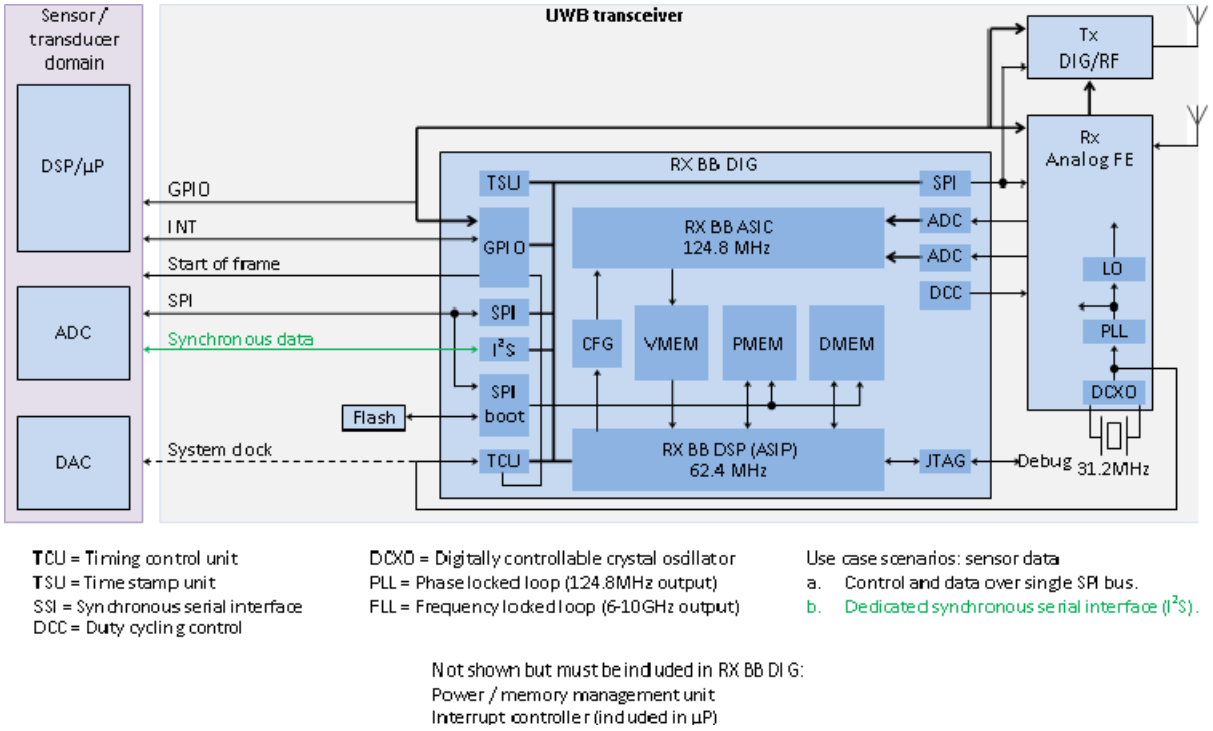

Figure 2.5: Transceiver block diagram (source: Holst Centre/imec)

2.2.1 Transmitter

The transmitter block diagram is shown in Figure 2.6. This block is responsible to generate the UWB packets from MAC data and transmit these packets. In the digital baseband section, the information is encoded as pulses with value $+1, -1$ or 0. These are translated into analog signals using the pulse generator. Together with a mixer, these blocks represent the transmitter modulator. The pulse amplitude can be controlled and the pulse duration can also be adjusted to some of the different IEEE 802.15.4a UWB pulse durations (Table 2.1). The differential output is fed into a differential antenna.

Bandwidth	**Pulse duration (T_p)**
499.2 MHz	2.0032 ns
1081.6 MHz	0.9246 ns
1331.2 MHz	0.7512 ns
1354.97 MHz	0.7380 ns

Table 2.1: IEEE 802.15.4a UWB pulse durations

2.2.2 Receiver

The coherent receiver architecture is shown in Figure 2.7. The differential signal, coming from the antenna is fed into a LNA. The output of the LNA is fed into two mixers,

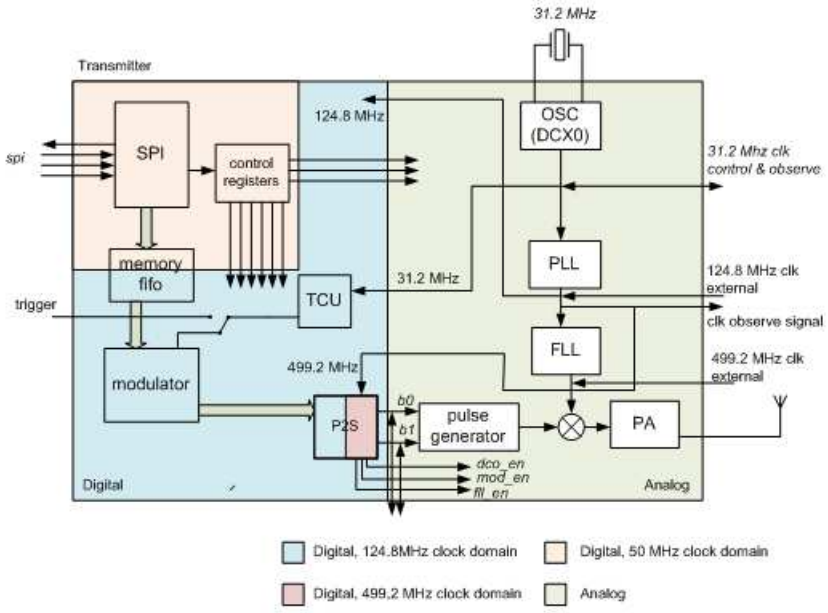

Figure 2.6: Transmitter block diagram (source: Holst Centre/imec)

one for the I (in phase) branch and one for the Q (quadrature) branch. These mixers have at their other input the UWB channel centre frequency (6-10 GHz). The mixer output is fed into a VGA which consists of an amplifying and filtering part. The outputs from the 5-bit Analog-to-Digital Converters (ADC) are further processed by the digital baseband (DBB) ASIC.

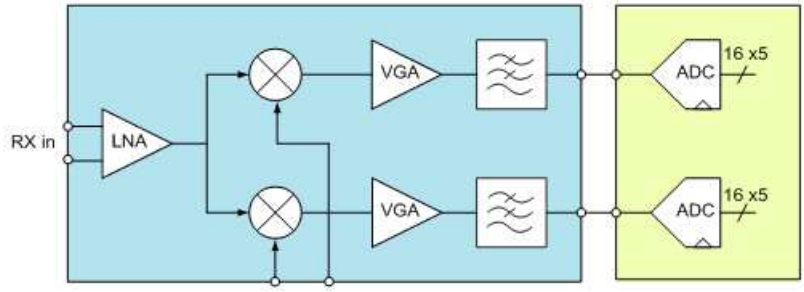

Figure 2.7: Coherent receiver architecture (source: Holst Centre/imec)

The application specific circuitry required to assist the UWB DSP is shown in Figure 2.8. The preamble detection and tracking are performed by the sub-sequence correlators and subsequent blocks, the PHR and payload are handled in the burst correlator and Rake detector block. For flexibility, the preamble detection stage can also use a magnitude input. The phase rotator in conjunction with the timing control block compensate for frequency offset by continuously adjusting the input phase.

The UWB frame construction is shown in Figure 2.9 indicating the processes required at each phase of the receiver operation. These processes are shared between the ASIC blocks and DSP software.

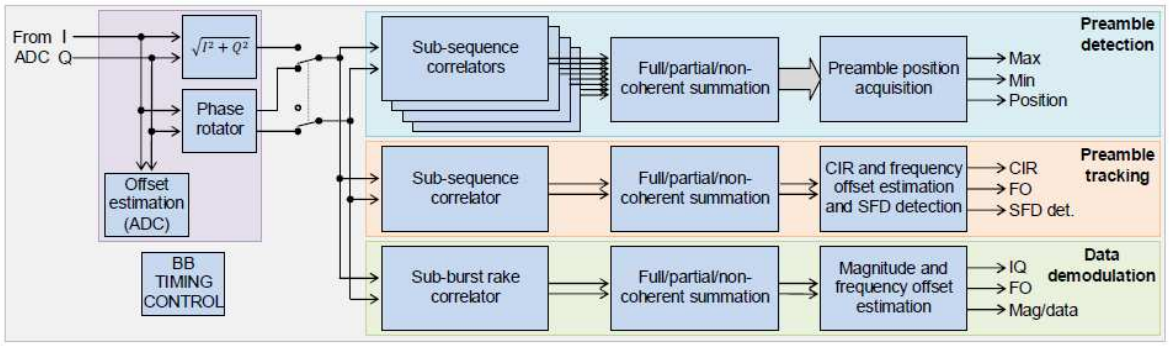

Figure 2.8: ASIC block (source: Holst Centre/imec)

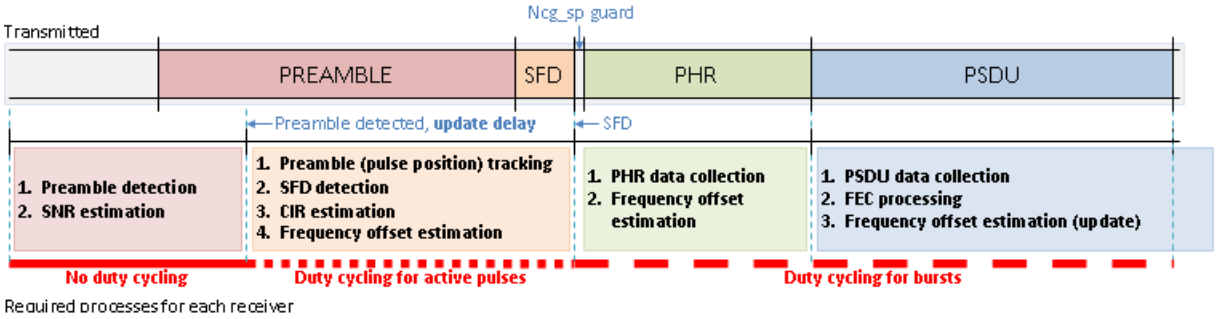

Figure 2.9: IEEE 802.15.4a Frame structure

Firstly, the receiver performs preamble detection wherein the receiver looks for the presence of a signal and then time aligns to the start of the preamble symbol. The estimation of the signal to noise ratio (SNR) is also done during this stage. A technique for this is described in chapter 4. This is followed by preamble tracking and SFD detection. A theoretical approach to setting the threshold for SFD detection is described in chapter 5. These are the two main operations that shall be described in this thesis.

Figure 2.10 shows the IR-UWB receiver with the digital baseband receiver implemented on a FPGA.

2.2.3 Types of detection

Due to the limits on emission levels of UWB signals, the received energy level is at or below noise level. To be able to detect pulses with such low energy, the receiver needs to combine multiple pulses. This is the reason for using special sequences with excellent autocorrelation properties for forming the preamble symbols. Correlation provides an improvement in the signal level.

Two methods of combining the signals are used: Coherent and Non-coherent. Non-coherent signal combination simply combines the energy of the samples. Coherent signal combination takes into account the phase of the signal by adding the samples vectorially. This has the advantage that the noise is suppressed and hence coherent

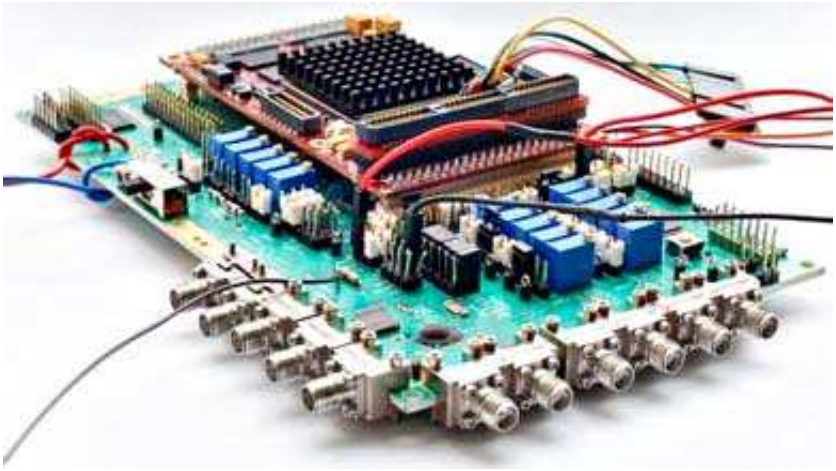

Figure 2.10: IR-UWB receiver developed by Holst Centre/imec

signal combination is assumed to offer superior performance compared to non-coherent detection.

In practice both transmitter and receiver will rely on some timing reference to generate the clock and carrier frequency. The signal generated by this references may deviate from the nominal frequency and it may fluctuate around its average frequency. The 802.15.4a standard allows a difference between the nominal and average frequency called the frequency offset, of up to 20 parts per million (ppm) [7]. The variance of the frequency deviation is known as jitter. The standard does not give any specifications for the jitter.

At baseband the frequency offset will cause a phase shift between successive samples. These phase shifts will affect receivers using coherent combination. Since the signal samples are not phase aligned, their sum will be smaller than expected. The phase shift may even go so high that the vectors add up destructively. In such a situation it is preferable to use non-coherent combining which discards the phase and uses only the magnitude. Thus the choice of using coherent or non-coherent depends on the extent of phase stability in the receiver.

3 Transmitter measurements

In this chapter, the IR-UWB transmitter is characterized in terms of output spectrum, channel power, bandwidth and DC power consumption. Compliance of average output power spectrum to the UWB transmit spectral mask is checked. An automated measurement setup is used which ensures that the settings are the same when measurements are repeated. Measurements are presented for mode 1.2 of the IR-UWB system.

3.1 Description of Setup

The transmitter (TX) measurement setup consists of three Printed Circuit Boards (PCBs), as shown in Figure3.1:

1. TX Pegasus V3.0, with both RF Front End (FE) and digital baseband (DBB) on one chip
2. Cepheus V1.0 124.8MHz and 499.2MHz clock generation board
3. Keil board for data transfer and Serial Peripheral Interface (SPI) control

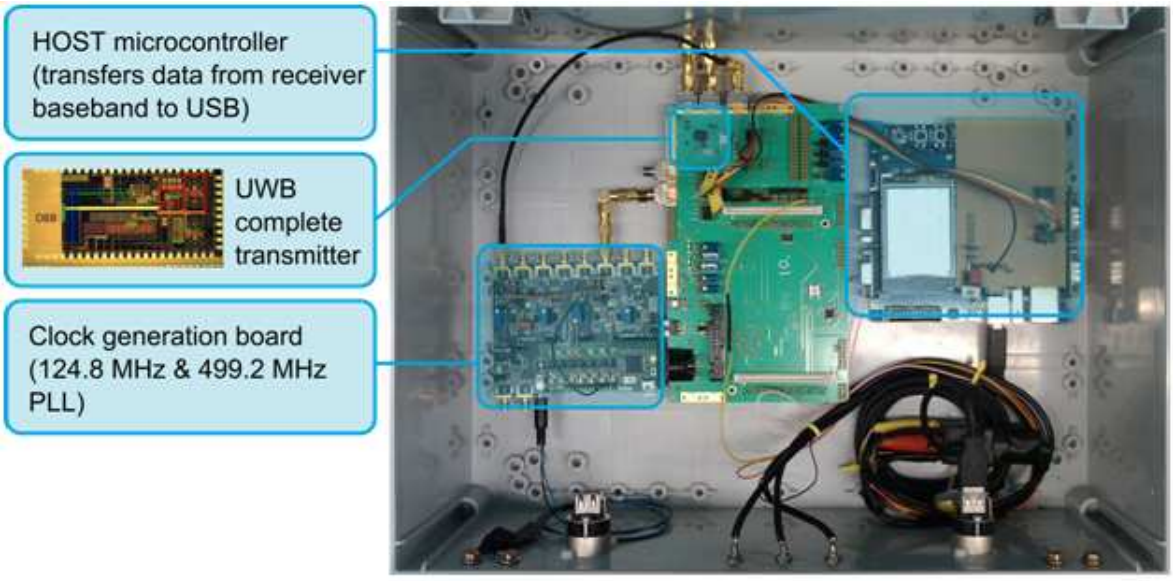

Figure 3.1: TX measurement setup

The TX block diagram is shown in Figure 3.2, including the RF FE and the digital baseband. The digital baseband needs two clock signals: 124.8 MHz and 499.2 MHz. The two clock signals can be supplied internally or externally.

For the internal case: the clock dividers need to be turned on (including the Current Mode Logic (CML) /2 divider, CML buffer and the True Single Phase Clocked (TSPC) /n divider chain). For the external case: the clock signals are generated by the clock board as shown in Figure 3.1, and the internal clock dividers can be turned off. As transmitter duty-cycling is not possible in the internal case, only the external case is considered in this report.

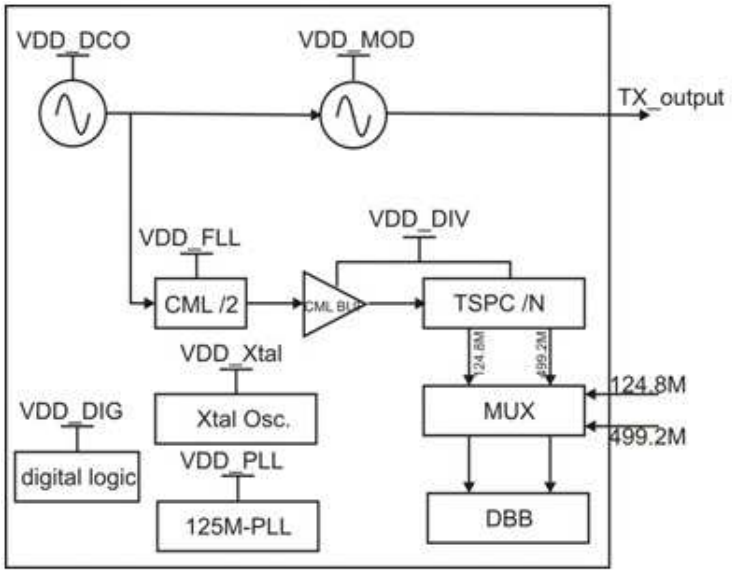

Figure 3.2: TX block diagram

The payload is an audio file which is transferred from a PC to the TX using the SPI interface of a Keil board. The differential output from the TX is fed to a spectrum analyzer/oscilloscope using a coaxial cable (pre-calibrated, cable+connector: 2.5 dB loss at 8 GHz).

The transmitter is capable of operating in a continuous mode and a duty-cycled mode. In the duty-cycled mode the TX modulator and digitally controlled oscillator (DCO) are duty-cycled i.e. switched off between the bursts of pulses and hence the average power consumption is lower compared to the continuous case.

The measurements are performed for Mode 1.2 of the IEEE 802.15.4a standard (Appendix A.1). This choice of mode was made after analysing the different modes on factors such as efficiency in DC power consumption and obtainable data rate. For the audio streaming application (eg. to a hearing aid), the lower data rate modes do not make sense as the required data rate cannot be achieved. The higher data modes lack in link-budget and this application requires a high link budget as the UWB signals have to go around the head (ear-to-ear communication). Between mode 1.2 and 2.2, the difference is not so big, although mode 1.2 has the advantage that with the same TX output power more link budget is obtained as there are more chips per burst in the PHR and PSDU. So, the measurements done using mode 1.2 are presented here. However, it is possible to do the measurements for the other modes as well using the automated measurement setup.

3.2 Transmit spectrum

The IEEE 802.15.4a standard specifies a transmit spectrum mask for the IR-UWB transmitter output [5]. The transmit power spectral density (PSD) mask requires that the transmitted PSD be less than -10 dBr (dB relative to the maximum spectral density of the signal) for $0.65/T_p < |f - f_c| < 0.8/T_p$ and -18 dBr for $|f - f_c| > 0.8/T_p$, where T_p denotes the pulse duration and is 2.003 ns corresponding to 499.2 MHz bandwidth when using the default pulse duration.

3.2.1 Automation of Measurements using MATLAB

The measurement of the transmitter output spectrum was automated using the General Purpose Interface Bus (GPIB) interface of the Agilent E4440 Spectrum Analyzer and controlled using the Instrument Control Toolbox of MATLAB.

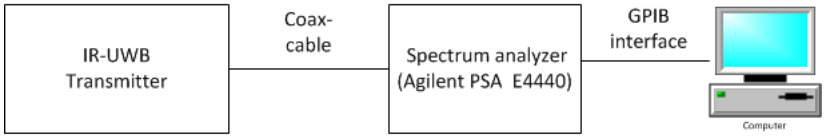

Figure 3.3: Transmitter spectrum measurement

3.2.2 Average Power

The measurement settings for the average power spectrum measurement using a spectrum analyzer are as specified in [8]:

1. Resolution Bandwidth, RBW=1 MHz
2. Video Bandwidth, VBW=3 MHz
3. Detector type: RMS
4. Sweep time 1 ms per spectrum point

Figure 3.4 shows the average power spectrum measured by setting 1 ms sweep time per spectrum point. But this results in a spectrum that is not smooth. This is caused by the frame-level duty-cycling, i.e. silent periods between frames (Figure 3.5). The period between start of frames is 2 ms, and effective duration of the frame in Mode 1.2 is 0.9 ms. The spectrum is calculated by averaging 1 ms sweep durations which result in different values when it is swept over the actual data and when it is in the silent portion between frames. This results in variations in the average spectrum.

Using a 2 ms sweep duration ensures that the full frame is covered and gives a smoother average spectrum plot as shown in Figure 3.6. The -10 dB bandwidth measured is greater than 500 MHz which satisfies the FCC requirement for UWB signals. From Figure 3.7 we can see that the UWB signal fits almost within the regulatory transmit spectrum mask.

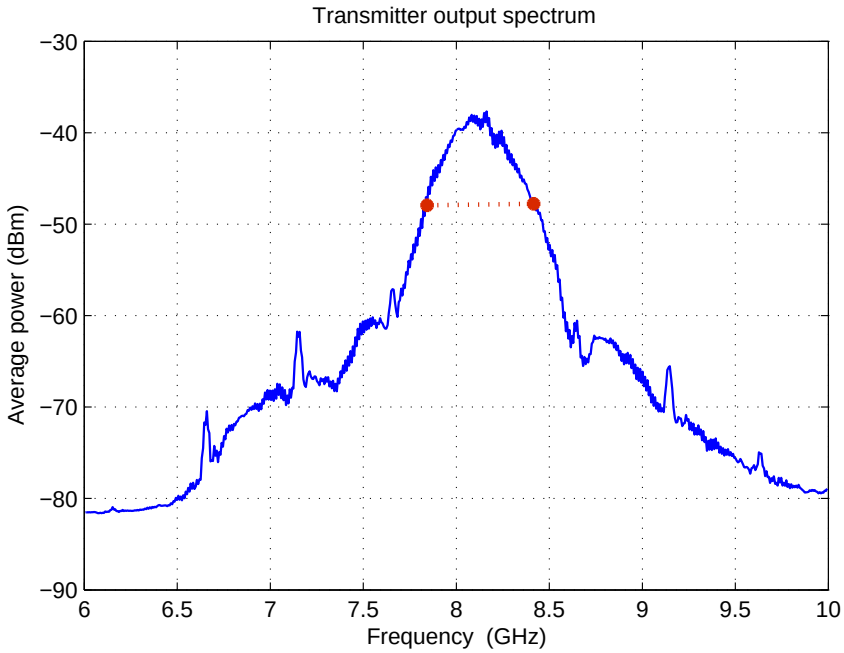

Figure 3.4: Average power spectrum measured in 1 MHz, 1 ms sweep time per point. The red line indicates the -10 dB bandwidth

Channel bandwidth (-10 dB) = 572.37 MHz
Centre frequency =8.13 GHz
Channel power (500 MHz BW) = -13.73 dBm

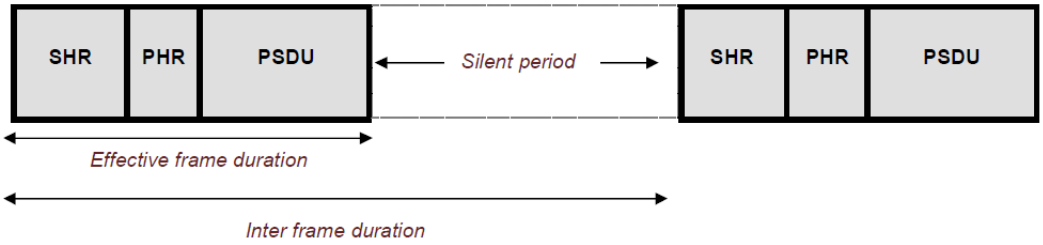

Figure 3.5: Frame-level dutycycling

The common pulse shapes used for low power IR-UWB topologies are: Trapezoidal, Exponential and Piece-wise Constant. The peak voltage of the UWB pulse can be evaluated from the average power measurement (P_{avg}) for these pulse shapes [9]. This is done by using the fourier transform of the time domain signal and calculating the average of the PSD in RBW around the RF carrier frequency. The average power depends on the peak voltage and the average pulse repetition frequency (PRF) of the mode. The peak voltage calculated from average power measurement is given by the

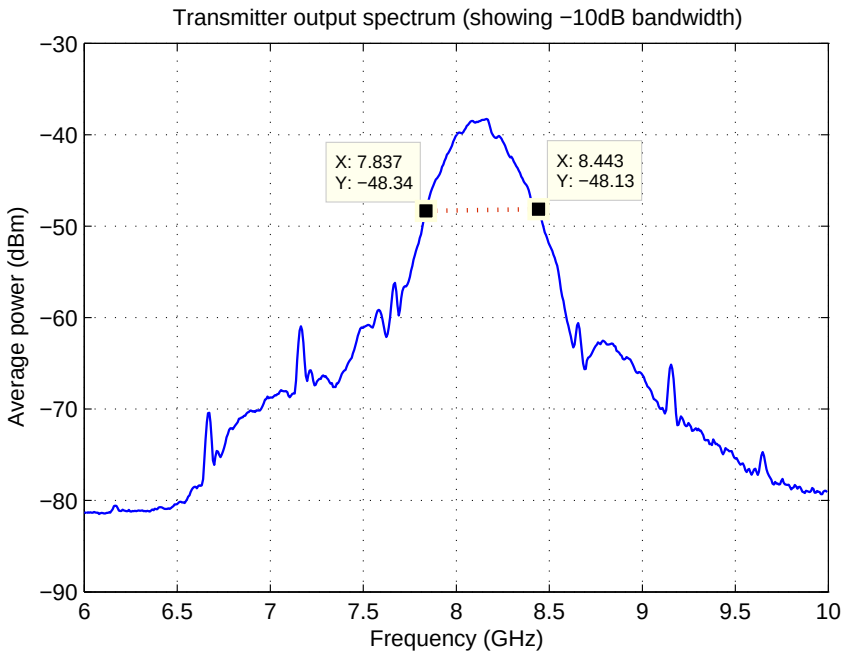

Figure 3.6: Average power measurement spectrum, measured in 1 MHz with sweep time 2ms per point in mode 1.2. The red line shows the -10 dB bandwidth

Channel bandwidth (-10 dB) = 605.65 MHz
Centre frequency =8.13 GHz
Channel power (500 MHz BW) = -13.66 dBm

relation [10]:

$$V_{pk} = \sqrt{\frac{P_{avg}\, 2\, Z_0}{PRF\, RBW\, \tau_{c,eff}^2}} \tag{3.1}$$

where
V_{pk} denotes the peak amplitude; P_{avg} is the average power (max value from average power PSD); PRF denotes the pulse repetition frequency (15.6 MHz for mode 1.2); RBW is resolution bandwidth (1 MHz); $\tau_{c,eff}$ is effective pulse width of single chip; Z_0 is characteristic impedance of antenna (50Ω).

This relation is computed assuming frames are continuous, i.e. there is no gap between frames. But since in the practical case there is a gap (silent period) between frames, we have to compensate for this frame level duty-cycling in the measured output power.

For mode 1.2 the frame level duty-cycle is 45%. This leads to a 3.4 dB reduction in the measured power. The maximum average power measured is -39 dBm in 1 MHz. Correcting for the 3.4 dB loss we get the P_{avg} as -35.6 dBm, which would have been the value measured has there been no gaps between frames. The peak voltage (V_{pk} calculated using 3.1 corresponding to this P_{avg} is 663 mV.

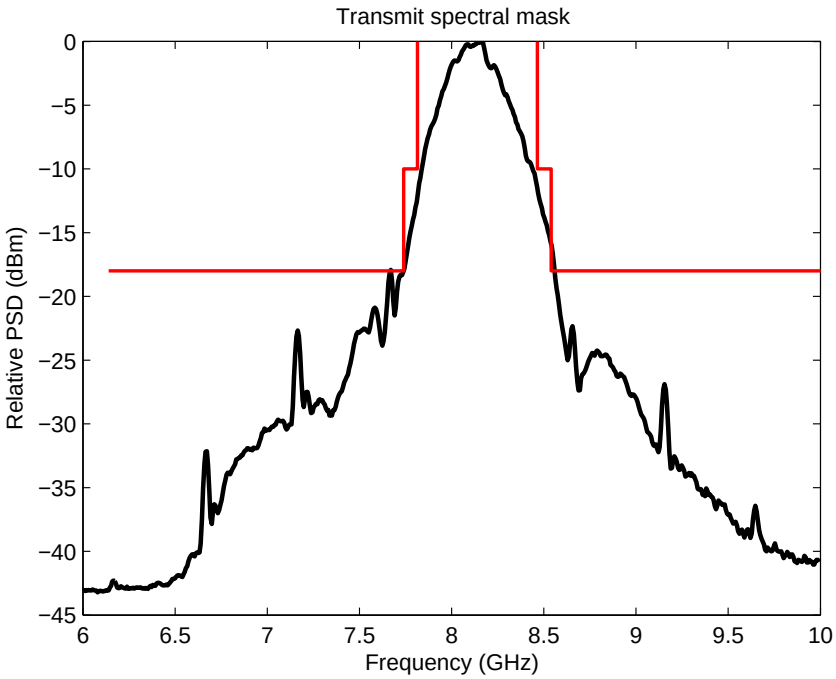

Figure 3.7: Transmitter output spectrum with IEEE 802.15.4a spectrum mask

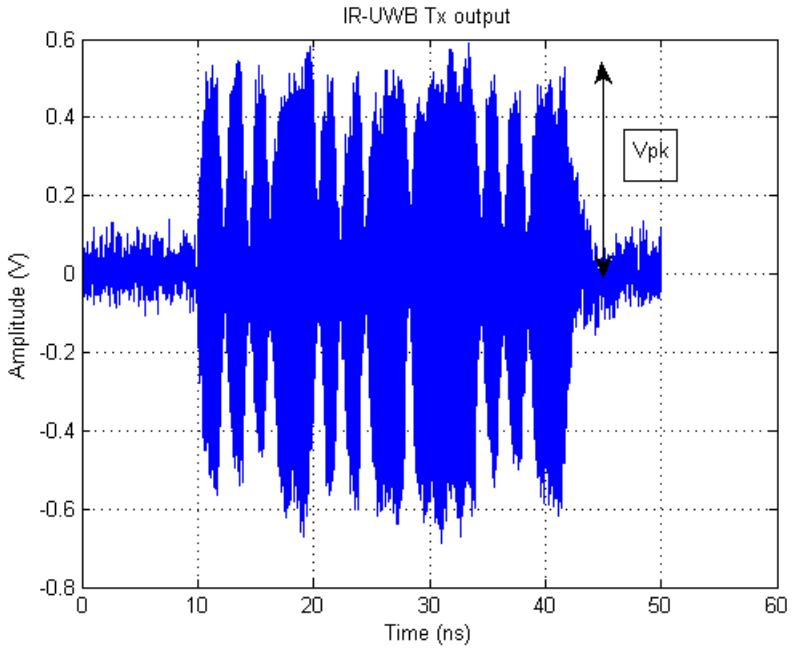

Figure 3.8: Measured burst using scrambling code with phase-inversions (captured on LeCroy serial data analyzer, 40 GS/s)

3.2.3 Peak Power

The peak PSD of an UWB transmission is the peak power referenced to a Gaussian filter of BW 50 MHz. The measurement is done using a peak detector and max hold [8]. Since most spectrum analyzers do not support a 50 MHz RBW, the highest RBW supported on the Agilent E4440 spectrum analyzer, i.e. 8 MHz, is used. The measured peak PSD is scaled to 50 MHz BW using a conservative scaling equation [8]:

$$Limit_{RBW} = Limit_{BW} + 20\,log_{10}(RBW/BW) \quad (in\ dBm) \tag{3.2}$$

where
RBW: resolution bandwidth (8 MHz); BW: bandwidth required (50 MHz)
$Limit_{RBW}$: Peak PSD in RBW ; $Limit_{BW}$: Peak PSD in BW

The spectrum analyzer measurement settings for the peak power measurement are:

1. RBW=8 MHz
2. VBW=8 MHz
3. Detector type: Peak
4. Max hold on

The peak power measurement can be performed using a spectrum analyzer (8 MHz RBW) with correction factor according to [9]. The transmitted peak power value can be extracted from a payload burst containing no phase changes, like the one shown in Figure 3.9. By disabling the LFSR feedback in the transmitter, each burst is coded without phase changes.

The peak voltage calculated from peak power measurement is given by the relation:

$$V_{pk} = \frac{\sqrt{P_{pk,b}\,2\,Z_0}}{\alpha_b} \tag{3.3}$$

where
V_{pk} denotes the peak amplitude; $P_{pk,b}$ is the peak power (max value from peak power PSD); α_b is the burst desensitization(BD) correction factor; Z_0 is characteristic impedance of antenna (50Ω).

$$\alpha_b = 1 - 2\,Q\left(\tau_{b,eff}, \sqrt{\frac{\pi}{2}}\,k_{pulse}\,50e6\right) \tag{3.4}$$

where
$\tau_{b,eff}$ denotes the effective burst width (32 ns); k_{pulse} relates the RBW of 50 MHz to an effective bandwidth for pulsed signals and is equal to 1.50797 for ideal Gaussian filter.

According to [10], the peak power value can be obtained through a frequency domain measurement using a spectrum analyzer with only 8 MHz bandwidth and using a correction factor. This requires that the time domain bursts have no phase inversions like the one shown in Figure 3.9. These bursts ensure a proper reading of peak power.

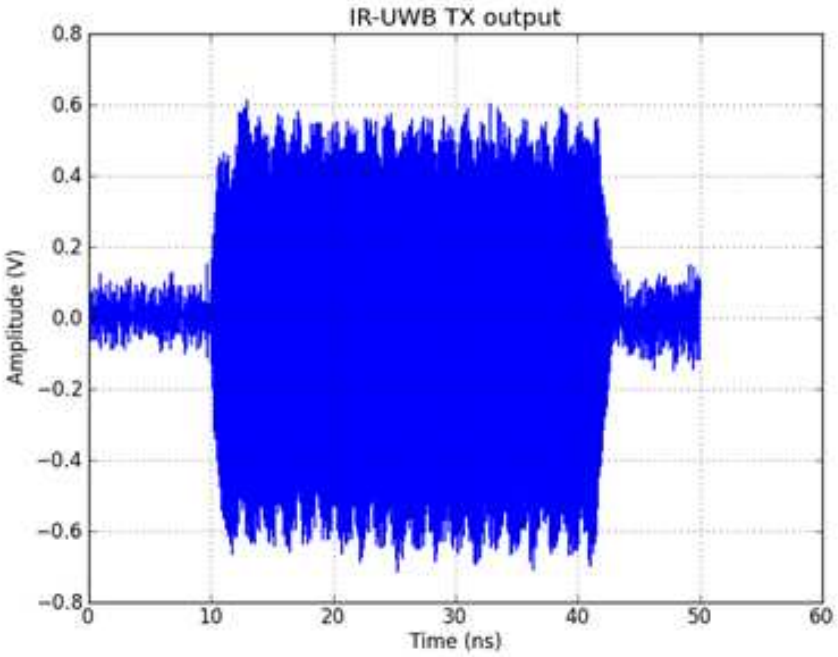

Figure 3.9: Measured burst using zero-phase-inversion scrambling code (captured on LeCroy serial data analyzer, 40GS/s)

From the spectrum analyzer measurement (Figure 3.10) a peak power value of -2.7 dBm in 8 MHz is read. Using Eq.3.2, this value is corrected to the required 50 MHz bandwidth value by adding $20\,log_{10}(50e6/8e6) = 15.9$ dB and subtracting (for 8 MHz and $\tau_{b,eff}$ of 32 ns) = 7.3 dB for the burst desensitization correction factor. This gives $-2.6+15.9-7.3 = 5.9$ dBm in 50 MHz. The 5.9 dBm peak power in 50 MHz corresponds to an effective amplitude,V_{pk} = 625 mV (using 3.3), which should correspond to an average output power of -36.1 dBm in 1 MHz using a 15.6 MHz PRF in Mode 1.2 (using 3.3). When post-processing the burst, using the time domain approach from [11], the peak power value of 5.5 dBm (in 50 MHz) is found, corresponding to an effective amplitude, $V_{pk} = 597$ mV for the 15.6 MHz PRF of the Mode 1.2 (expressions are summarized in appendix A.2).

The effective amplitude calculated using the peak power spectrum measurement (625 mV) is close to that observed on the oscilloscope (597 mV). The measured average output power is -35.6 dBm in 1 MHz which is close to the expected value of -36.1 dBm in 1 MHz, computed from the peak power measurement. The peak voltage measured using average power measurement (663 mV) is slightly higher than the expected value (597 mV). This is because the average power spectrum is not exactly flat around the centre frequency, there are slight variations. Thus, peak power measurement gives a more reliable estimate for the peak voltage compared to average power measurement.

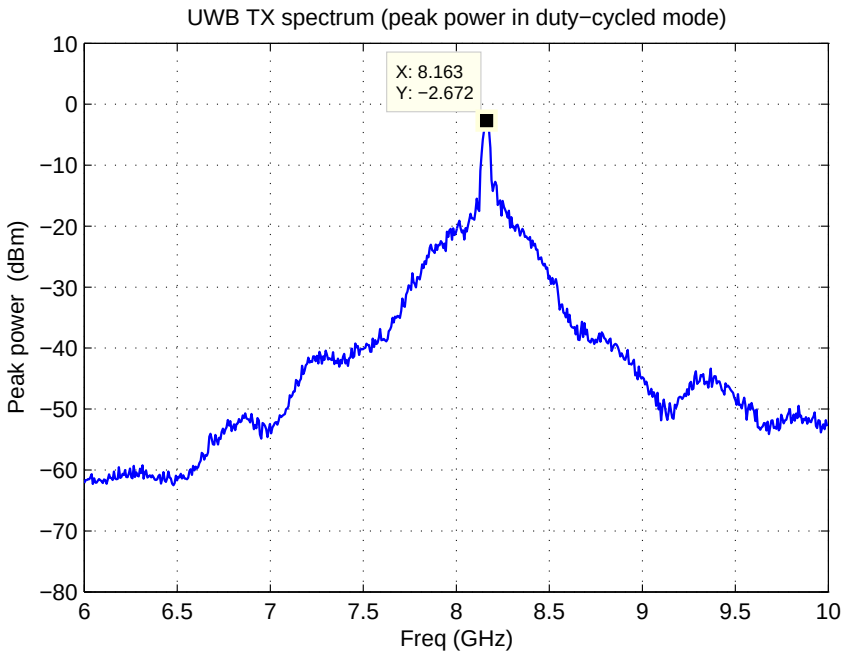

Figure 3.10: Measured peak power spectrum (dBm) in 8 MHz of a complete frame consisting of bursts having no phase changes. For this measurement a spectrum analyzer is used (frequency domain measurement)

3.3 Pulse shape

The current implementation of the UWB transmitter uses an exponential pulse shape, which can be described as

$$y = \begin{cases} 1-exp(-\frac{t}{\tau}) & 0 \leq t \leq T_p \\ exp(-\frac{(t-T_p)}{\tau}) - exp(-\frac{T_p}{\tau}) & t > T_p \end{cases} \tag{3.5}$$

where y denotes the envelope of the pulse; t is time; τ is the time-constant; T_p is pulse duration (2.003 ns)

The time-constant of the pulse is related to the pulse duration (T_p). By overlapping the measured pulse with the pulse shape (Figure 3.11) it is found that $\tau = 0.3\,T_p$. The time constant of the pulse can be controlled by the pulse shaping circuit (Figure 3.12).

Varying the bias current and load capacitance modifies the time constant. The effect on the spectrum -10 dB bandwidth is shown in Figure 3.13. In the default setting the bias current is set to minimum and load capacitance is set to maximum. The figure shows that this setting is the optimum setting for the output spectrum to fit within the TX mask.

3.4 DC Power consumption

The power consumption of the transmitter is measured in the following cases:

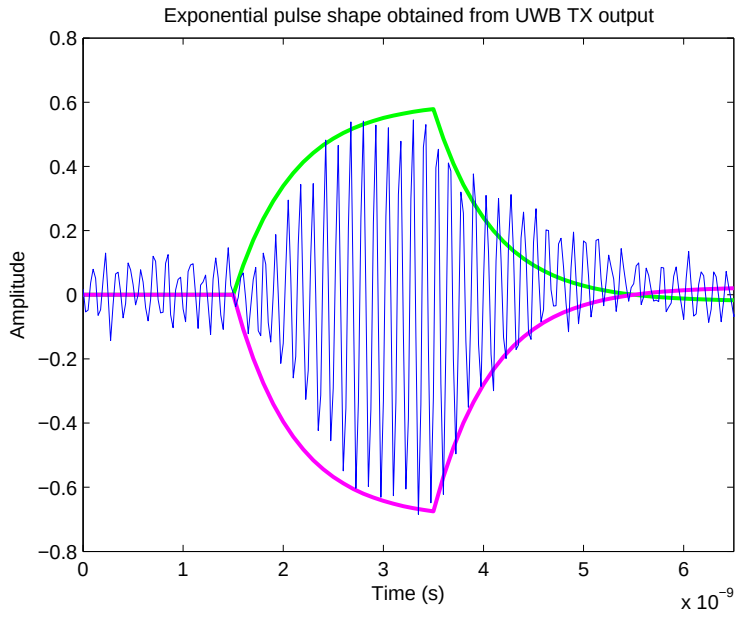

Figure 3.11: Exponential pulse (captured using Lecroy oscilloscope)

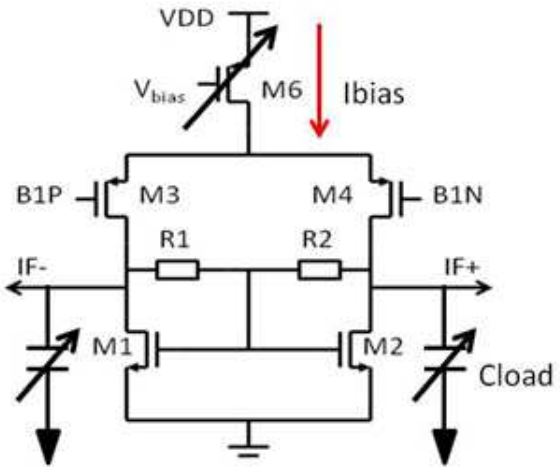

Figure 3.12: RC pulse-shaping circuit in TX

1. Off: all the blocks are switched off by the internal SPI interface
2. Continuous: All the blocks are turned on, while the divider chain is switched off i.e. VDD_FLL and VDD_DIV are zero
3. Duty-cycle: All the blocks are duty-cycled, while the divider chain is switched off

Measuring the DC power consumption in a continuous mode of operation is straightforward: measure the supply voltage and multiply with the measured current consumption. The typical mode of operation of an IR-UWB radio is in a duty-cycled mode.

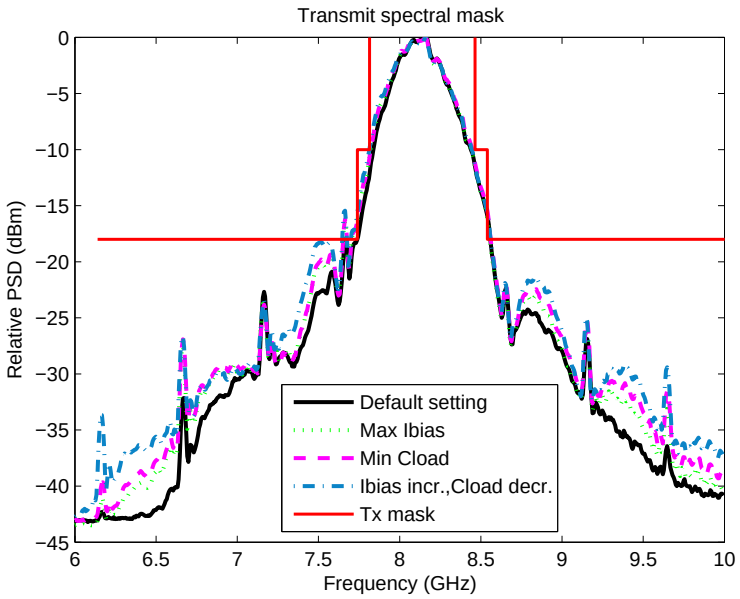

Figure 3.13: Relative PSD with varying register settings for bias current and load capacitance

This means the current consumption is also not time-constant. This current is measured using a Keithley 2400 meter.

On the transmitter board the following DC power consumption values are measured.

State	**Value**	**Unit**
DCO+TX modulator	4.80	mA
DCO only	4.28	mA
TX modulator only	4.42	mA
All off	3.66	mA

Table 3.1: DC current measurement: duty cycled mode, divider switched off

In table 3.1, the relatively high leakage current of 3.66 mA is mainly caused by the divider in off state. All values are measured when the voltage entering the board is set to 1.2 V.

State	**Value**	**Unit**
DCO+TX modulator	54.6	mA
DCO only	36	mA
TX modulator only	27.6	mA
All off	3.66	mA

Table 3.2: DC current measurement: continuous mode, divider switched off

Comparing the average current values for the continuous and duty-cycled mode from the tables,subtracting the leakage current, we see that current in the continuous mode is $54.6 - 3.66 = 50.94$ mA and in duty-cycled mode it is $4.80 - 3.66 = 1.14$ mA. Thus duty-cycling reduces power consumption by a factor of $\frac{50.94}{1.14} \approx 45$.

3.5 Summary

Measurements of the IR-UWB transmitter were performed for mode 1.2.

- The transmitter output spectrum fits almost within the transmit spectrum mask and the channel bandwidth is greater that 500 MHz as required for a UWB signal.
- The peak voltage calculated using the peak power measurement using a spectrum analyzer matches with the peak voltage calculated using the burst of pulses measured on the oscilloscope.
- The effect of varying the pulse shaping parameter on the output spectrum is observed and the best setting is selected.
- From the DC power consumption measurements it is observed that DC power consumption in duty-cycled mode is considerably lower (factor of 45) than in the continuous case.

4 Preamble detection

In this chapter, firstly, the method used for detection of the Synchronisation Header (SHR) preamble is explained. Expressions for the probability distributions of the outputs of the preamble detection block are derived for both coherent and non-coherent cases. Since the IR-UWB system is a pulse based system, the pulse level signal to noise ratio is an important indicator of the received signal power. A method to estimate the received signal-to-noise ratio (SNR) per pulse from the preamble correlator output is proposed this chapter.

4.1 Introduction

Preamble detection is required to determine the presence and timing position of the preamble. The synchronisation header (SHR) preamble consists of SYNC and SFD portions. The SYNC portion is made of repeated preamble symbols (S_i), each symbol takes elements from the ternary (+1, -1 and 0) code sequence (C_i) and inserts ($N_{cpp} - 1$) zeros between each element, where N_{cpp} is the chips per pulse. The number of SYNC and SFD symbols, N_{cpp}, length and sequence of C_i are adjustable. Preamble detection relies on correlation to increase the SNR. The receiver is continuously on during the preamble detection stage i.e. duty-cycling is not possible.

Figure 4.1 shows the preamble detection block. The incoming chip sequence (samples) is correlated with the ternary preamble sequence (0, +1 or -1). The preamble detection hardware uses sub-correlators for correlation. The sub-sequence approach has advantages over the normal correlation detector in terms of memory access rate (from the delay line) and power consumption. The incoming chips are written to the delay line, the sub-sequences are calculated by reading 6 taps from the delay line and the current input. For a given ternary sequence, the sub-sequences and delay required between the sub-sequences are defined. The sequences are correlated coherently or non-coherently (only magnitude used). The magnitude of the correlator output is computed and accumulated for a fixed number of times (L) using an accumulator.

For a preamble sequence of length C_{len} and chips per pulse N_{cpp}, the number of possible positions (N) is given by $N = C_{len}\, N_{cpp}$, which corresponds to the number of chip durations per preamble symbol (S_i). For $C_{len} = 31$ and $N_{cpp} = 16$ the number of chip positions is 31x16 = 496. At the end of L symbol accumulations, the maximum and minimum values from set of accumulator outputs of all chip positions and the position of the maximum value are stored.

The outputs of the preamble correlation block, thus, are (Figure 4.1): the Max

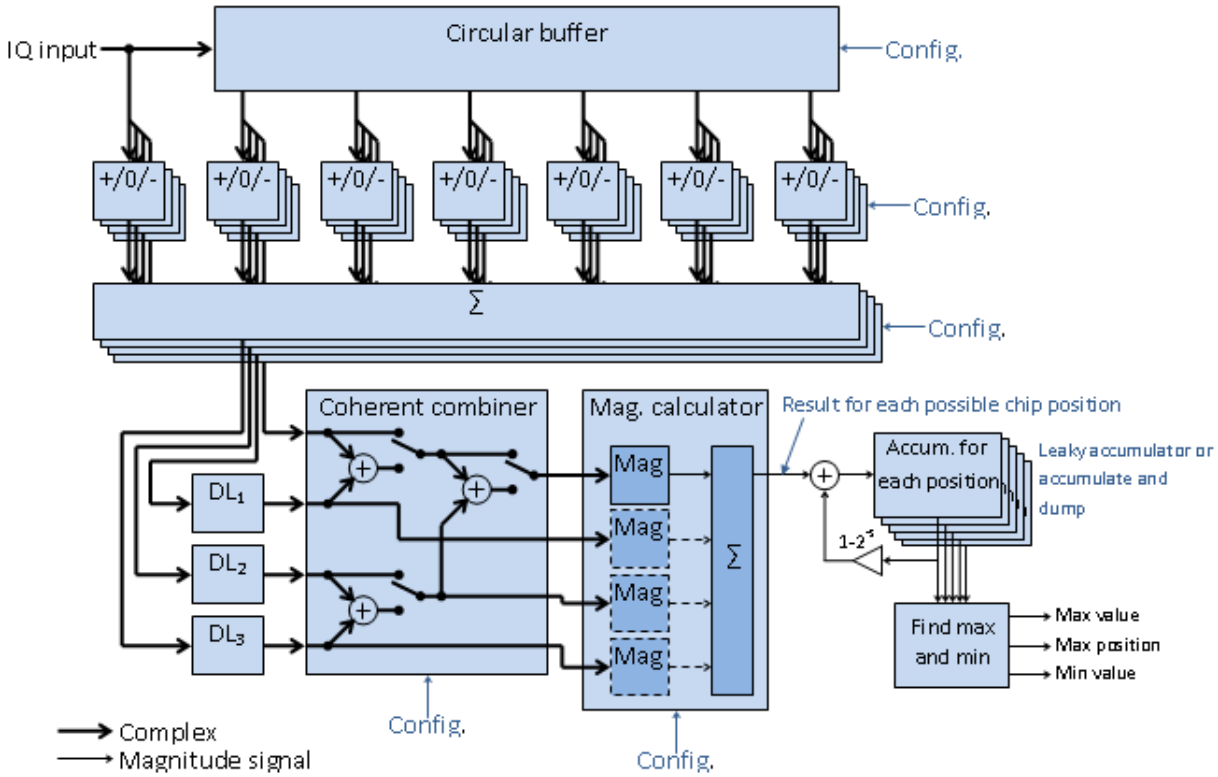

Figure 4.1: Preamble correlation block (source: Holst Centre/imec)

value, which we shall denote as *max*, position of *max* and the Min value, which we shall denote as *min*. Although for detecting the preamble, the maximum value and the index of the maximum value are sufficient, the min value was also included as it is easy to compute in the hardware.

For our analysis we consider length 31 preamble code sequence i.e. $C_{len} = 31$. Figure 4.2 lists some of the preamble codes.

Code index	Ternary sequence	Four zero aligned sequence
1	-0000+0-0+++0+-000+-+++00-+0-00	0000+0-0+++0+-000+-+++00-+0-00-
2	0+0+-0+0+000-++0-+---00+00++000	0000+0+-0+0+000-++0-+---00+00++
3	-+0++000-+-++00++0+00-0000-0+0-	0000-0+0--+0++000-+-++00++0+00-
4	0000+-00-00-++++0+-+000+0-0++0-	0000+-00-00-++++0+-+000+0-0++0-
5	-0+-00+++-+000-+0+++0-0+0000-00	0000-00-0+-00+++-+000-+0+++0-0+
6	++00+00---+-0++-000+0+0-+0+0000	0000++00+00---+-0++-000+0+0-+0+
7	+0000+-0+0+00+000+0++---0-+00-+	0000+-0+0+00+000+0++---0-+00-++
8	0+00-0-0++0000--+00-+0++-++0+00	0000--+00-+0++-++0+000+00-0-0++

Figure 4.2: List of all the length 31 preamble codes in the standard

It can be observed that all C_i sequences have 4 consecutive zeros. Since the zeros do not affect the result of the correlation, discarding them does not change the output. Since we have four sub-correlators each of length 7, we require 4x7 = 28 coefficients. Therefore the 28 coefficients are taken from the zero-aligned sequence, starting at the coefficient after the four consecutive zeros, discarding three of the four zeros. As an example, the four sub-sequences obtained using preamble code index 3 of Figure 4.2 are given below,

Subsequence[1]= [-1 0 +1 0 -1 -1 +1]
Subsequence[2] = [0 +1 +1 0 0 0 -1]
Subsequence[3]= [+1 -1 +1 +1 0 0 +1]
Subsequence[4] = [+1 0 +1 0 0 -1 0]

The SHR preamble is said to be detected when the following conditions are satisfied:

- Comparison test

  To check if the max is above the threshold.

  $$max(n) > \lambda\, min(n)$$

  where n denotes the nth output value from the preamble detection block, λ is a multiplier of min which serves as a threshold.

- Consistency check for max position

  To ensure that the position of max is the same for successive symbols.

  $$Index(n) = Index(n-1) = Index(n-2) = ...Index(n-conf)$$

  where $Index$ denotes the position of the max and $conf$ is the number of confirmations required for fixing the position of the preamble.

4.2 Coherent case

In the coherent case, the incoming samples are multiplied with the ternary C_i coefficients and fed to a summation unit. The outputs of the sub-sequence correlators are also combined coherently.

For the coherent case, during preamble correlation in the absence of noise, a peak is obtained when the preamble code coefficients are aligned exactly over the start of the symbol, and otherwise the result is zero as shown in Figure 4.3. When additive white gaussian noise (AWGN) is added, the amplitudes of the received samples are Gaussian distributed. Since correlation is a linear operation, the outputs of the correlation are also Gaussian distributed [12]. We get a non-zero mean Gaussian variable corresponding to the correlation peak and a zero-mean Gaussian variable otherwise. The preamble

code sequence C_i of length 31 consists of 16 non-zero values (8 '+1's and 8 '-1's). Hence, the correlation output distribution is given by,

$$Peak \sim N(16\,A, \sigma_o^2) + j\,N(16\,A, \sigma_o^2) \tag{4.1}$$

$$Sub - peaks \sim N(0, \sigma_o^2) + j\,N(0, \sigma_o^2) \tag{4.2}$$

where A is the amplitude of the samples and $\sigma_o^2 = 16\,\sigma^2$, σ^2 is the noise variance per chip in either branch (I or Q).

The magnitude of the output is used in accumulation. The envelope of a non-zero mean Gaussian distributed variable has a Rician distribution and the envelope of a zero-mean Gaussian variable has a Rayleigh distribution [12]. The distribution of the correlation output is thus Rician or Rayleigh depending on whether it is the correlation peak or noise. After accumulation, the distribution of the correlation output for each possible chip position is 'Sum of Rician' or 'Sum of Rayleigh' (Figure 4.4).

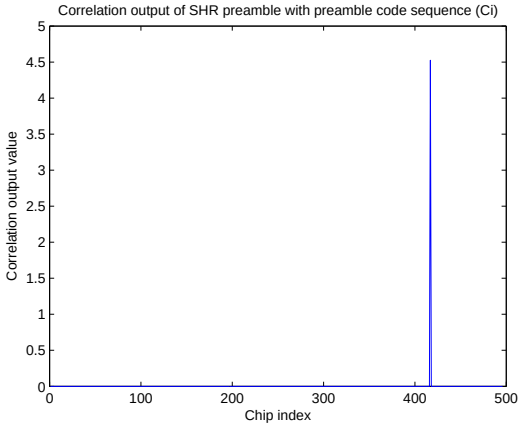

Figure 4.3: Preamble correlation for L=2 accumulations, no noise

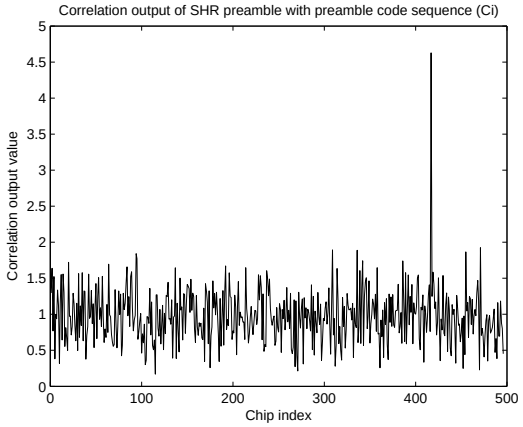

Figure 4.4: Preamble correlation for L=2 accumulations, adding noise

4.2.1 Distribution of Max

Let $X = [x_1, x_2, x_3.....x_N, x_{peak}]$ denote the set of accumulator outputs where x_i are Rayleigh distributed (or sum of Rayleigh for accumulated case i.e. $L > 1$) i.i.d variables and x_{peak} denotes the correlation peak which is Rician distributed (or sum of Rician for $L > 1$).

$$p(max(X) = y) = \sum_{1}^{N+1} p(x_n = y)\,P(X_{others} < y) \tag{4.3}$$

$$p(max(X) = y) = N\,p_x(x_1 = y)F_X(y)^{N-1}F_{X_{peak}} + p_{X_{peak}}(x_{peak} = y)F_X(y)^N \tag{4.4}$$

For $L = 1$ case,

$$p_X(y) = \frac{y}{\sigma_o^2}\, exp\left(\frac{-y^2}{2\,\sigma_o^2}\right) \text{ (Rayleigh distribution)}$$

$$F_X(y) = 1 - exp\left(\frac{-y^2}{2\sigma_o^2}\right)$$

$$p_{X_{peak}}(y) = \frac{y}{\sigma_o^2}\, exp\left(\frac{-(y^2+16\,A^2)}{2\,\sigma_o^2}\right)\, I_0\left(\frac{16\,A\,y}{\sigma_o^2}\right) \text{ (Rice distribution)}$$

$$F_X(y) = Q_1\left(\frac{16\,A}{\sigma_o}, \frac{y}{\sigma_o}\right)$$

(Refer to Appendix A.3 for Rice and Rayleigh distribution expressions)

For $L > 1$, we require the PDF and CDF of the 'Sum of Rician' variables, a closed form expression of which is not available. So the distribution of *max* cannot be expressed in closed form either, as it depends on the distribution of the 'Sum of Rician' variables.

But it is known that in case of a correct detection, the *max* corresponds to the correlation peak which has a Rician distribution (or 'Sum of Rician' distribution for the case when $L > 1$). In case of an incorrect detection, one of the noise samples has magnitude higher than the actual correlation peak. In this case, *max* is Rayleigh distributed for $L = 1$ or 'Sum of Rayleigh' distributed for $L > 1$.

4.2.2 Estimating SNR in the coherent case

The signal to noise ratio per pulse (SNR) is defined as follows:

$$SNR = \frac{A^2}{\sigma_c^2} \tag{4.5}$$

where A is the pulse amplitude, and $\sigma_c^2 = 2\,\sigma^2$ denotes the total noise variance.

It has been shown that the noise variance can be estimated in the preamble detection stage. The description of the technique is skipped here due to confidentiality reasons.

In case of correct detection, *max* corresponds to the correlation peak which has a:

- Rician distribution: $Rice(16\,A, \sigma_o)$ for number of accumulations, $L = 1$
- Sum of Rician distribution: $\sum_{i=1}^{L} Rice(16\,A, \sigma_o)$ for $L > 1$

Using the mean and variance of *max* and the estimated noise variance, the pulse amplitude A can be estimated. The expressions for mean and variance of Rician variables is given in Appendix A.3.

$$E(peak^2) = \frac{1}{L}\, variance(max) + (\frac{1}{L}\, E(max))^2 \tag{4.6}$$

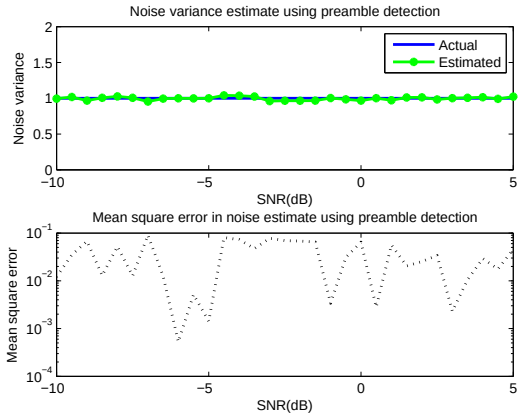

Figure 4.5: Noise estimate in coherent case (statistics using 100 values)

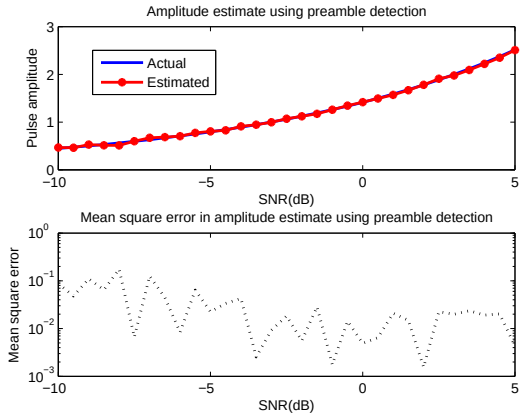

Figure 4.6: Amplitude estimate in coherent case (statistics using 100 values)

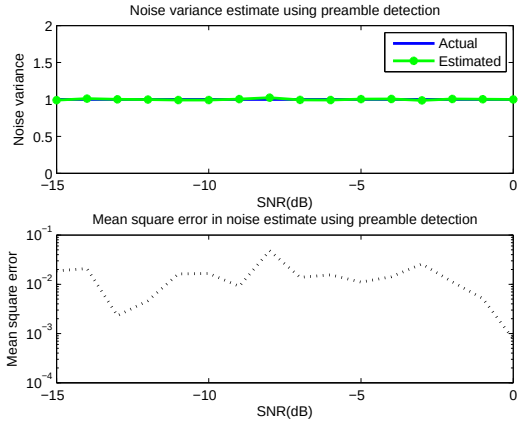

Figure 4.7: Noise estimate in coherent case (statistics using 1000 values)

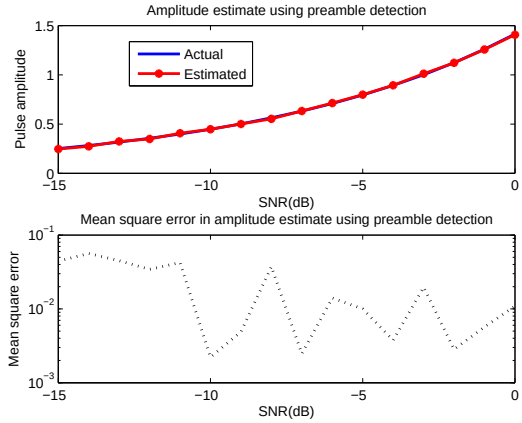

Figure 4.8: Amplitude estimate in coherent case (statistics using 1000 values)

Here we use the property that the mean and variance of sum of variables is the sum of the individual means and variances respectively of the variables. The mean and variance are scaled by the number of accumulations (L) to obtain the second moment ($E(peak^2)$) of the correlation peak. This is used to get an expression for the amplitude estimate,

$$\widehat{A} = \frac{1}{16}(E(peak^2) - 2\,\widehat{\sigma_o}^2) \tag{4.7}$$

where $\widehat{A}$ denotes the amplitude estimate; $\widehat{\sigma_o}^2$ denotes the estimated noise variance.

Figures 4.5, 4.6, and 4.9 show the noise variance, amplitude and SNR estimates obtained from the statistics of 100 output values as an example. Using more values

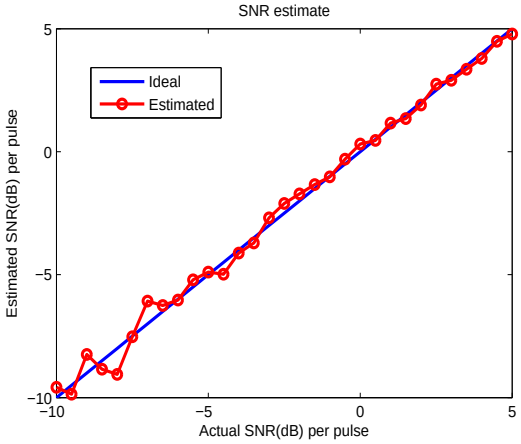

Figure 4.9: SNR estimate in coherent case (statistics using 100 values)

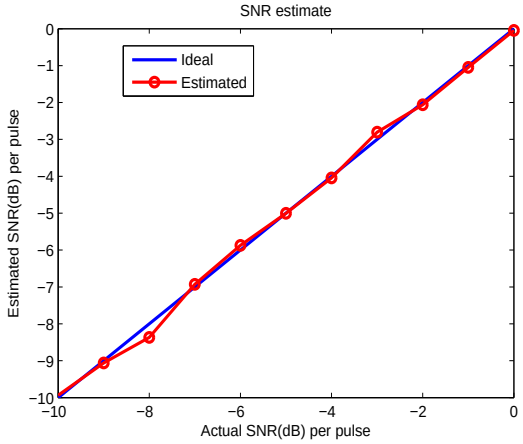

Figure 4.10: SNR estimate in coherent case (statistics using 1000 values)

results in a better estimation i.e. lower mean square error (MSE) in the estimates, as shown in Figures 4.7, 4.8 and 4.10.

4.2.3 Number of frames required: an example

In the coherent case, the number of output values required for estimation of the amplitude ans noise with mean square error (MSE) less then 10^{-1} is about 100. Better accuracy can be obtained by using larger number of output values. The output values are available every L symbols where L is the number of accumulations. Consider a SHR preamble of length 64 which consists of 64 SYNC symbols and 8 SFD symbols. Since only the SYNC symbols are used for preamble detection, the number of outputs available per frame considering L=4, is $(\frac{64}{4}) = 16$ values. So the number of correct ("good") frames required for estimation is $\frac{100}{16}$ which is about 7. This number is smaller for longer SHR preamble lengths (1024 or 4096 symbols).

4.3 Non-coherent case

In the non-coherent case, the magnitude of the incoming sequence is multiplied with the modified version of ternary C_i coefficients and fed to a summation unit. Two options are available for this,

- Unsigned coefficients
  In this case, the ternary coefficients (0,+1,-1) are converted to binary (0,1) using

$$C_i^{'} = |C_i| \tag{4.8}$$

  i.e. +1,-1 becomes 1 and 0 is unchanged.

- Signed coefficients
  In this case, the ternary coefficients (0,+1,-1) are converted to binary (-1,1) using

$$C_i' = 2\,|C_i| - 1 \tag{4.9}$$

  i.e. +1,-1 becomes 1 and 0 becomes -1.

From Figures 4.13 and 4.13, it can be observed that the cross-correlation sub-peaks have a relatively higher value compared to the sub-peaks when using the signed coefficients. In the unsigned case, of the 28 coefficients 16 are '1's and 12 are '0's. The zeros play no role in correlation output. However when using signed coefficients, the '0' s become '-1's and these negative coefficients play a role in reducing the amplitude of the cross-correlation sub-peaks.

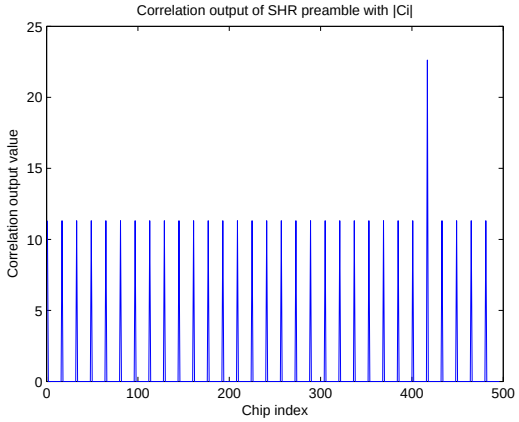

Figure 4.11: Non-coherent preamble correlation for L=2 accumulations using unsigned coefficients, no noise

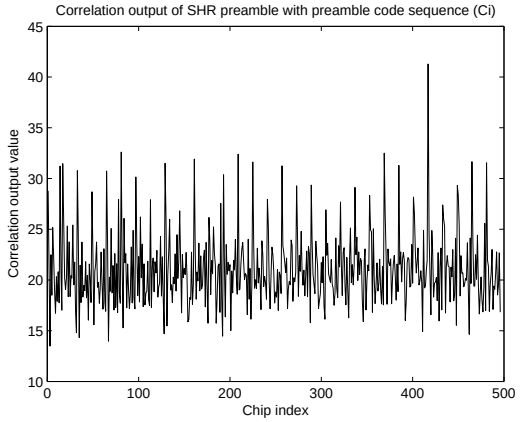

Figure 4.12: Non-coherent preamble correlation for L=2 accumulations using unsigned coefficients, adding noise

For the non-coherent case, in the absence of noise, the output of the correlation is the highest peak corresponding to the start of the preamble symbol, smaller peaks at positions which are multiples of N_{cpp} (i.e. 16 in our case) and zero otherwise. In the presence of additive white gaussian noise (AWGN), after taking the magnitude of the received samples, each of the samples is Rician/Rayleigh distributed depending on whether the mean is non-zero or zero.

- For +A,-A the distribution is $Rice(A, \sigma)$ with mean and variance denoted by μ_{rice} and σ^2_{rice}
- For 0 the distribution is $Rayleigh(\sigma)$ with mean and variance denoted by $\mu_{rayleigh}$ and $\sigma^2_{rayleigh}$.

During correlation, these samples are multiplied by the coefficients and summed. The output of the preamble correlation thus has a 'Sum of Rayleigh/Rician distribution. The correlation output is then input to the accumulator. The *max* value, position of *max* value and *min* value are obtained from the accumulator output.

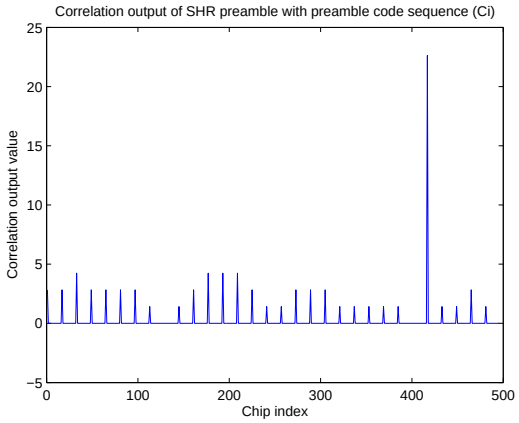

Figure 4.13: Non-coherent preamble correlation for L=2 accumulations using signed coefficients, no noise

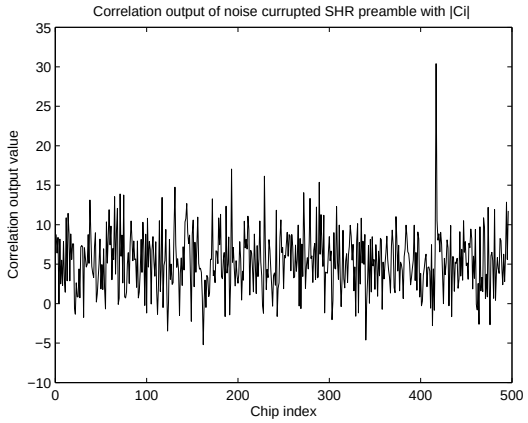

Figure 4.14: Non-coherent preamble correlation for L=2 accumulations using signed coefficients, adding noise

4.3.1 Estimating the SNR in non-coherent case

It has been shown that the noise variance can be estimated in the preamble detection stage in the non-coherent case. The description of the technique is skipped here due to confidentiality reasons.

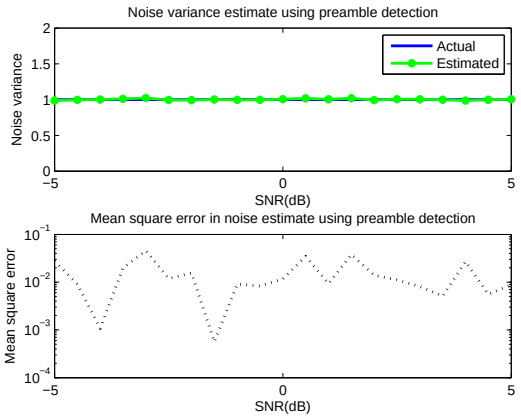

Figure 4.15: Noise estimate in non-coherent case (statistics using 1000 monte-carlo runs)

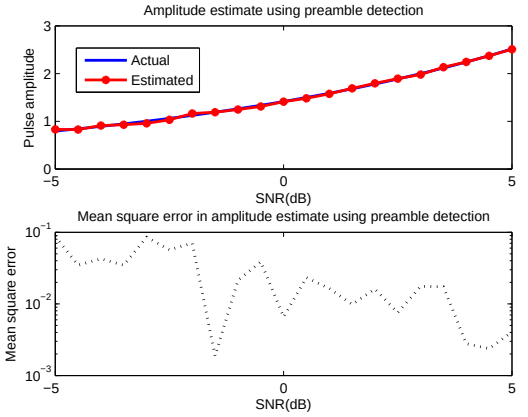

Figure 4.16: Amplitude estimate in non-coherent case (statistics using 1000 monte-carlo runs)

In case of correct detection, *max* corresponds to the correlation peak (or sum of peaks) which has a distribution:

$$\text{Accumulator output} \sim \sum_{i=1}^{16} Rice(A,\sigma) - \sum_{i=1}^{12} Rayleigh(\sigma) \text{ for } L = 1$$

$$\text{Accumulator output} \sim \sum_{1}^{L}[\sum_{i=1}^{16} Rice(A,\sigma) - \sum_{i=1}^{12} Rayleigh(\sigma)] \text{ for } L > 1$$

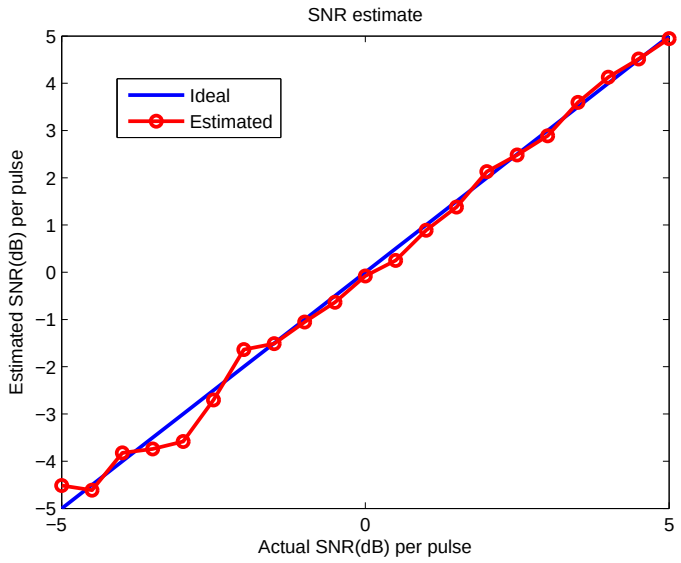

Figure 4.17: SNR estimate in non-coherent case (statistics using 1000 monte-carlo runs)

Using the mean and variance of max the pulse amplitude A can be estimated. The expressions for mean and variance of Rician variables is given in Appendix A.3.

$$E(max) = L\,(16\,\mu_{rice} - 12\,\mu_{rayleigh}) \tag{4.10}$$

$$var(max) = L\,(16\,\sigma^2_{rice} + 12\,\sigma^2_{rayleigh}) \tag{4.11}$$

Using these equations, and solving for A we get,

$$\widehat{A} = \sqrt{\frac{1}{16}\,[\frac{1}{L}(var(max) + \frac{1}{16}(E(max) + 12\sqrt{\frac{\pi}{2}}\widehat{\sigma})^2) - (56 - 6\,\pi)\widehat{\sigma^2}]} \tag{4.12}$$

where $\widehat{A}$ denotes the amplitude estimate; $\widehat{\sigma^2}$ denotes the noise variance estimate.

Figures 4.5, 4.6, and 4.9 show the noise variance, amplitude and SNR estimates with mean squared error less than 10^{-1}, obtained from the statistics of 1000 output values as an example.

4.3.2 Number of frames required: an example

In the non-coherent case, the number of output values required for estimation of the amplitude and noise with mean square errors (MSE) less then 10^{-1} is about 1000. The output values are available every L symbols where L is the number of accumulations. Consider a SHR preamble of length 64 which consists of 64 SYNC symbols and 8 SFD symbols. Since only the SYNC symbols are used for preamble detection, the number

of outputs available per frame considering L=4, is $(\frac{64}{4}) = 16$ values. So the number of frames required for estimation is $\frac{1000}{16}$ which is about 63 frames. This number is smaller for longer SHR preamble lengths.

4.4 Summary

In this chapter, the preamble detection process in the IR-UWB system was described. A method to estimate the signal-to-noise ratio per pulse (SNR) using the outputs of the preamble detection block was proposed.The SNR information is useful for in further stages (SFD detection, demodulation) of the receiver.

5 SFD Detection Analysis

In this chapter, detection of the Start of Frame Delimiter (SFD), which marks the start of the payload, is described. A mathematical approach to determine the optimal detection threshold is derived for the coherent and non-coherent cases. The detection performance using the derived threshold is compared to the current implementation.

5.1 Introduction

SFD detection is important to establish frame timing [5]. It is preceded by preamble detection step, which informs the start of the symbol time to the receiver.

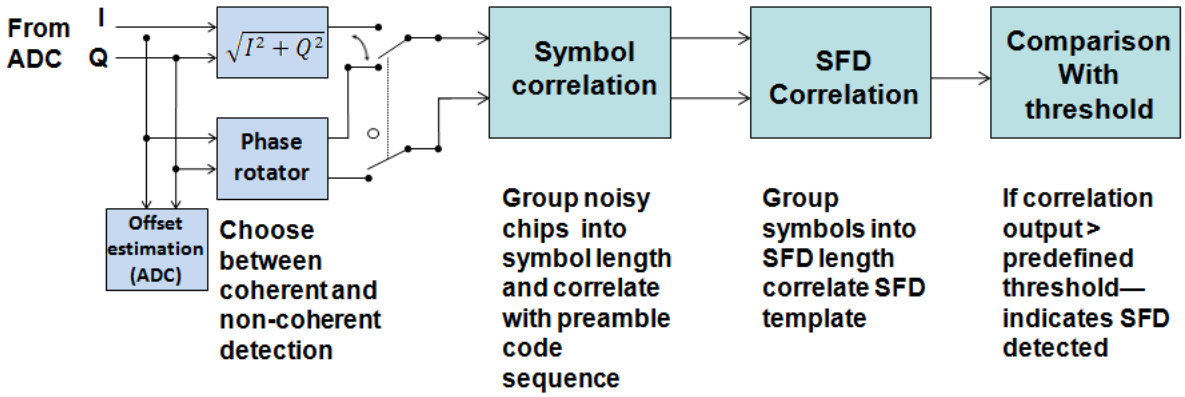

Figure 5.1: SFD detection block diagram

The received signal is converted to baseband by the analog front end. The baseband signal is sampled at the chip rate (499.2 MHz) to obtain the chip sequence. For the analysis, it is assumed that the UWB pulses are sampled at the peak points to obtain the samples. The received chip sequence is corrupted by noise. As shown in Figure 5.1, the Analog to Digital Convertor (ADC) gives both I and Q components. The receiver, then searches for a start frame delimiter (SFD) code that indicates the start of the payload data and this process is termed SFD detection. Figure 5.1 illustrates the various steps in the SFD detection stage.

5.1.1 Current implementation

In the current implementation, initially the threshold is set to an arbitrarily high value. An SFD detection timeout event implies a missed SFD due the threshold being too high and if the payload decoding fails it means it was a false detection i.e. the threshold is too low. So the threshold is gradually adjusted to balance both these opposing events.

When there is a detection, the maximum and second maximum of the SFD correlation outputs are stored. By computing the statistics (mean, variance) of the maximum and second maximum of the SFD correlation outputs (see Figure 5.2) during detections, a suitable threshold is computed. This method of threshold setting does not take into account the actual distributions of the correlation outputs and also large number of frames are wasted before a suitable threshold is determined. Therefore a theoretical approach is required.

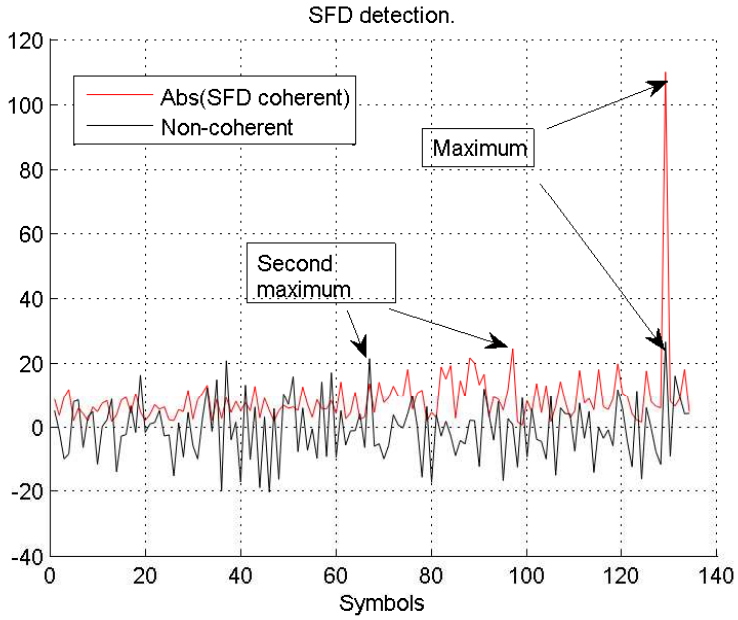

Figure 5.2: SFD correlation output with noise

For SFD detection, the probability distributions corresponding to the SFD peak and the secondary peaks which arise from cross-correlation with the non-SFD portion of the preamble, need to be derived. Using these distributions an analytical threshold that maximises the detection probability can be determined.

5.2 System model

Samples/Chips: ternary (+A, -A, 0) denoted by a_i, where A denotes the received pulse amplitude.

The signal to noise ratio per pulse (SNR) is given by,

$$SNR = \frac{A^2}{\sigma_c^2} \tag{5.1}$$

where A denotes the pulse amplitude and $\sigma_C^2 = \sigma_R^2 + \sigma_I^2 = 2\,\sigma^2$ denotes the total complex noise variance which is the sum of the equal variances of the I and Q components.

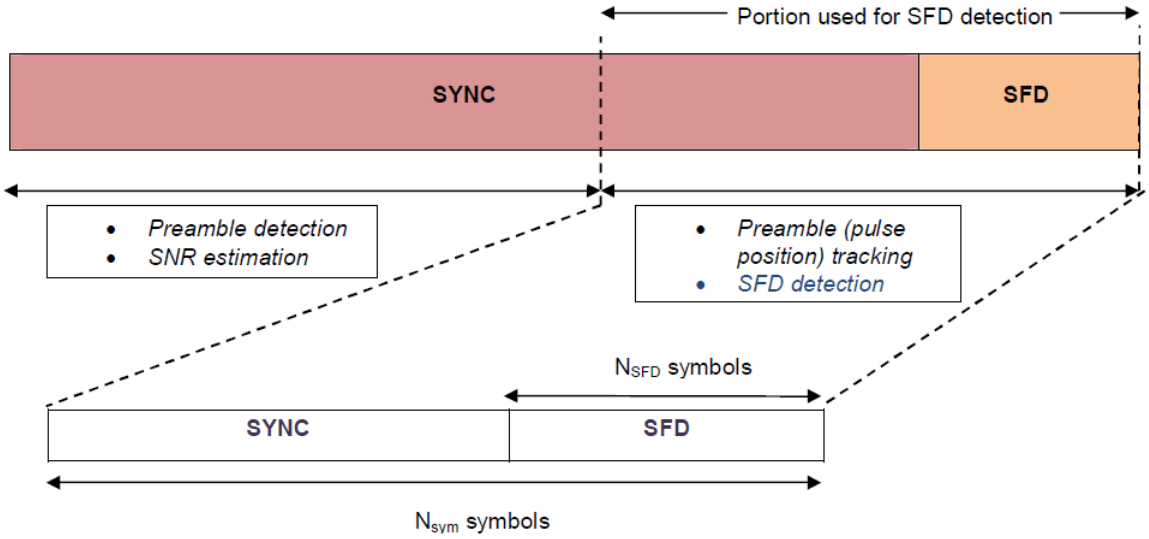

Figure 5.3: SHR preamble

Let the received samples after addition of white gaussian noise (AWGN) be denoted by $NoisyChips$. The probability distribution of the received samples ($Noisychips$) is Complex Gaussian as given below,

$$Noisychips \sim N(a_i\, cos(\phi), \sigma^2) + j\, N(a_i\, sin(\phi), \sigma^2) \tag{5.2}$$

with $N(\mu, \sigma^2)$ denoting a Gaussian distribution with mean μ and variance σ^2 and ϕ denotes the carrier phase.

5.3 Coherent case

In coherent detection, the phase information of the samples is used in the detection process. The symbols are obtained by coherent combination of the samples.

5.3.1 Symbol correlation

Let N_{sym} denote the total number of preamble symbols used in SFD detection (see Figure 5.3). Each preamble symbol S_i consists of $C_{len} * N_{cpp}$ chip positions. After preamble detection, the start of the symbol is known and hence the $N_{cpp} - 1$ zeros inserted between each preamble code value can be neglected to get the required samples. In the symbol correlation step, the received samples are grouped into symbol lengths (i.e. C_{len}) to obtain $Symbolchips$. In order to obtain the symbol, $SymbolChips$ is correlated with the known C_i sequence.

$$CohSym(n) =< SymbolChips(n), C_i > \tag{5.3}$$

where $CohSym$ denotes the coherently obtained symbol and $n \in [1, N_{sym}]$

The preamble code sequence C_i is a ternary sequence with very good auto-correlation properties. The length 31 sequence consists of sixteen non-zero terms (8 '+1's and 8 '-1's) and fifteen '0's. The SYNC part of the preamble is just a repetition of the C_i sequence. So de-spreading using C_i gives a result of $K = 16\,A$, where the 16 comes from the number of non-zero terms in the C_i code and A is the received pulse amplitude.

Using (5.2), the distribution of coherently obtained symbols is given by,

$$CohSym(n) \sim N\left(16\,A\,cos(\phi), 16\,\sigma^2\right) + j\,N\left(16\,A\,sin(\phi), 16\,\sigma^2\right) \tag{5.4}$$

The SFD part of the SHR preamble is the length N_{SFD} ternary sequence spread by the C_i sequence. So multiplication of an SFD symbol with C_i i.e. $a_i\,c_i$ gives +K, -K or 0 depending on the sign of the SFD term.

Thus, for non-zero SFD symbols (i.e. +1 or -1),

$$CohSym(n) \sim N\left(\pm 16\,A\cos(\phi), 16\,\sigma^2\right) + j\,N\left(\pm 16\,A\,sin(\phi), 16\,\sigma^2\right) \tag{5.5}$$

And for '0 terms of SFD, the distribution is the sum of the noise distribution,

$$CohSym(n) \sim N\left(0, 16\,\sigma^2\right) + j\,N\left(0, 16\,\sigma^2\right) \tag{5.6}$$

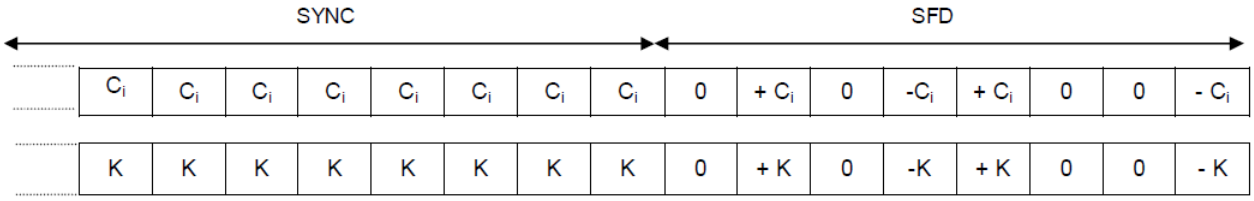

Figure 5.4: SHR preamble symbols without adding noise; (*above*) before symbol correlation and (*below*) after symbol correlation

5.3.2 SFD correlation

For detecting the SFD, the obtained symbols are correlated with the known SFD sequence template. The SFD peak after correlation marks the detection of the SFD. The SFD sequence is a ternary sequence (+1,-1 or 0) of length 64 (or 8).

Let the output of SFD correlation be denoted by Sf. Sf is obtained as the result of correlating the SFD template with the received SHR preamble symbols as shown in Figure 5.6. Thus, $Sf\,(1)$ gives the result of correlation of symbols 1 to N_{SFD} with the SFD template, $Sf\,(2)$ gives the result of correlation of symbols 2 to $N_{SFD}+1$ and so on. Since there are N_{sym} symbols, the number of correlation outputs is $N_{sym} - N_{SFD} + 1$.

$$Block(n) = [CohSym(n), CohSym(n+1)...CohSym(n+N_{SFD}-1)] \tag{5.7}$$

$$Sf(n) =< Block(n), SFD > \tag{5.8}$$

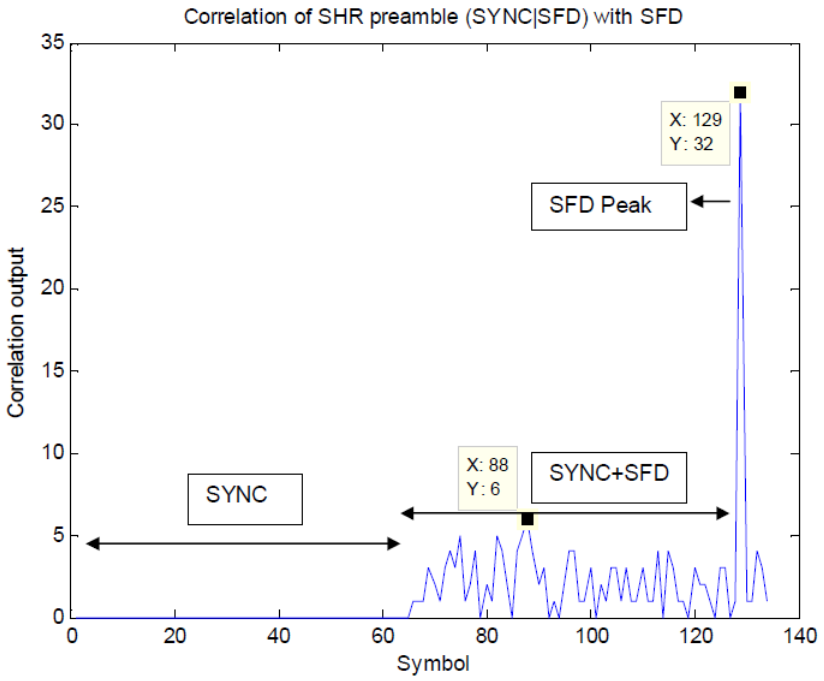

Figure 5.5: SFD correlation output (y) in coherent case

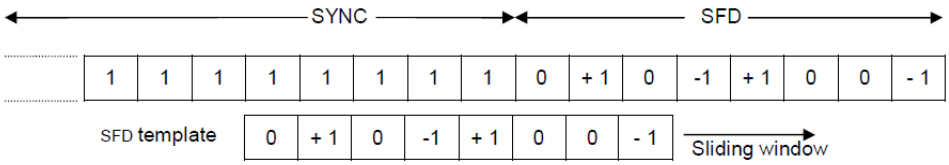

Figure 5.6: Cross-correlation of SHR preamble with the SFD sequence (without adding noise)

where $1 \leq n \leq N_{sym}$.

Figure 5.5 shows the cross-correlation outputs of the SHR preamble symbols with the SFD sequence for N_{sym} =196 ans N_{SFD} =64.

Let denote the terms of the SFD. the The SFD sequences are constructed such that $\sum SFD(i) = 0$. Out of the N_{SFD} symbols in SFD, $N_{SFD}/2$ symbols are non-zero and others are zeros. The result of the correlation depends on which portion of the SHR preamble is taken, i.e. SYNC, SYNC+SFD or only SFD. So, in the following, they are analysed separately.

5.3.2.1 SYNC portion

The SYNC portion of the SHR preamble consists of repetition of the S_i symbols. So despreading gives a constant value for all symbols. Since the SFD sequence has equal number of '+1's and '-1's, the correlation result is zero. In the presence of AWGN noise the correlation output has a complex gaussian distribution.

The mean and variance (of the I/Q component) of the resulting distribution are given by,

$$E[Sf(k)] = 0 \tag{5.9}$$

$$Var[Sf(k)] = 16 \left(\frac{N_{SFD}}{2} \right) \sigma^2 \tag{5.10}$$

where $k \in$(SYNC), and the $\left(\frac{N_{SFD}}{2}\right)$ term corresponds to the number of non-zero terms in the SFD sequence template.

The distribution of the correlation output of this portion is thus,

$$Sf(k) \sim N \left(0, 16 \frac{N_{SFD}}{2} \sigma^2 \right) + j\, N \left(0, 16 \frac{N_{SFD}}{2} \sigma^2 \right) \tag{5.11}$$

The magnitude of the correlation output has a Rayleigh distribution given by,

$$|Sf(k)| \sim Rayleigh \left(\sqrt{16 \frac{N_{SFD}}{2} \sigma^2} \right) \tag{5.12}$$

5.3.2.2 SYNC+SFD portion

In this case the non-coherent symbols of the tail of SYNC and the initial part of the SFD is correlated with SFD template sequence. In the absence of noise, let the output of cross-correlation with the ith block starting at symbol index i be denoted by $y(i)$ where $i \in$(SYNC+SFD) (Figure5.5).

The output y is obtained assuming that the mean of the symbols is unity. After symbol correlation, the obtained corrupted by noise have a distribution as given in (eq:cohsym distribution). The mean and variance (of the I/Q component) are obtained as,

$$E[Sf(i)] = (16\, A\, cos(\phi))\, y(i) \;\; or \;\; (16\, A\, sin(\phi))\, y(i) \tag{5.13}$$

$$Var[Sf(i)] = 16 \left(\frac{N_{SFD}}{2} \sigma^2 \right) \tag{5.14}$$

The distribution of the ith correlation output of this portion is thus given as,

$$Sf(i) \sim N \left(y(i)(16\, A\, cos(\phi)), 16 \frac{N_{SFD}}{2} \sigma^2 \right) + j\, N \left(y(i)\, (16\, A\, sin(\phi)), 16 \frac{N_{SFD}}{2} \sigma^2 \right) \tag{5.15}$$

where $i \in$(SYNC+SFD)

The magnitude of the correlation output in this portion has a Rice distribution given by,

$$|Sf(i)| \sim Rice \left(16\, A\, y(i), \sqrt{16 \frac{N_{SFD}}{2} \sigma^2} \right) \tag{5.16}$$

5.3.2.3 SFD correlation peak

In this case the coherent SFD symbols are correlated with SFD template giving the correlation peak. In the presence of AWGN noise, the correlation output is Gaussian distributed.

The mean and variance (of the I/Q component) are given by,

$$E[Sf(peak)] = \left(\frac{N_{SFD}}{2}\right) 16\, A\, cos(\phi) \;\; or \;\; \left(\frac{N_{SFD}}{2}\right) 16\, A\, sin(\phi) \tag{5.17}$$

$$Var[Sf(peak)] = 16 \left(\frac{N_{SFD}}{2}\right) \sigma^2 \tag{5.18}$$

The distribution of the correlation output of this portion is thus given by,

$$Sf(peak) \sim N\left(\frac{N_{SFD}}{2} 16\, A\, cos(\phi), 16\, \frac{N_{SFD}}{2}\, \sigma^2\right) + j\, N\left(\frac{N_{SFD}}{2} 16\, A\, sin(\phi), 16\, \frac{N_{SFD}}{2}\, \sigma^2\right) \tag{5.19}$$

The magnitude of the correlation output peak has a Rician distribution given by,

$$|Sf(peak)| \sim Rice\left(\frac{N_{SFD}}{2} 16\, A, \sqrt{16\, \frac{N_{SFD}}{2}\, \sigma^2}\right) \tag{5.20}$$

5.3.3 Evaluation of threshold

The SFD detection process encounters a false alarm when one or more of the side-peaks, caused by cross correlation of noise corrupted SHR preamble with SFD template sequence, crosses the threshold. A missed detection occurs when an actual SFD peak is lower than the threshold. The total error probability is thus the sum of the probability of false alarm and probability of missed detection.

The optimal threshold is chosen such that it maximizes the detection probability (P_d).

$$\begin{aligned} P_d &= (1 - P_{fa})\,(1 - P_{miss}) \\ &= (1 - Prob\,(side - peaks > threshold))\,(1 - Prob\,(SFDpeak < threshold)) \end{aligned} \tag{5.21}$$

In the previous section, the distributions of the SFD correlation outputs were derived. Out of the $N_{sym} - N_{SFD} + 1$ outputs, $N_{sym} - N_{SFD}$ outputs correspond to the side peaks and the final term is the SFD correlation peak. A false alarm occurs when any of the cross-correlation side-peaks (SYNC and SYNC+SFD portions) crosses above the threshold i.e. if one of the side-peaks or a combination of them is above the threshold. Alternatively, a false alarm does not occur if all the side-peaks have an amplitude less

than the threshold. The probability of false alarm can thus be expressed as one minus the probability that all the side-peaks are less than threshold.

$$P_{fa} = 1 - \prod_{i=1}^{N_{sym}-N_{SFD}} P(Sf(i) < threshold) \tag{5.22}$$

The probability that a random variable is less than or equal to a specific value is given by its cumulative distribution function (CDF). Hence the term in the product can be rewritten using the CDF of the variable. Since, all the correlation outputs are Rician distributed, the CDF is given by the Marcum-Q function.

$$P_{fa} = 1 - \prod_{i=1}^{N_{sym}-N_{SFD}} \left(1 - Q_1\left(\frac{4\,A\,y_i}{\sqrt{\frac{N_{SFD}}{2}}\,\sigma}, \frac{\gamma}{4\sqrt{\frac{N_{SFD}}{2}}\,\sigma}\right)\right) \tag{5.23}$$

where γ denotes the threshold, $Q_1(a, b)$ denotes the Marcum-Q function.

The missed detection probability is the probability of the SFD peak begin less than the threshold, which is given by its CDF,

$$P_{miss} = 1 - Q_1\left(\frac{\sqrt{\frac{N_{SFD}}{2}}\,4\,A}{\sigma}, \frac{\gamma}{4\sqrt{\frac{N_{SFD}}{2}}\,\sigma}\right) \tag{5.24}$$

where γ denotes the threshold.

Combining both,the detection probability is given by,

$$P_d(\gamma) = \left(\prod_{i=1}^{N_{sym}-N_{SFD}} \left(1 - Q_1\left(\frac{4\,A\,y_i}{\sqrt{\frac{N_{SFD}}{2}}\,\sigma}, \frac{\gamma}{4\sqrt{\frac{N_{SFD}}{2}}\,\sigma}\right)\right)\right)\left(Q_1\left(\frac{\sqrt{\frac{N_{SFD}}{2}}\,4\,A}{\sigma}, \frac{\gamma}{4\sqrt{\frac{N_{SFD}}{2}}\,\sigma}\right)\right) \tag{5.25}$$

The threshold γ is chosen such that it maximizes P_d.

Taking the derivative of P_{miss} w.r.t γ from (5.23), we get the PDF of the SFD peak.

$$p_{peak}(\gamma) = \frac{\gamma}{16\,(\frac{N_{SFD}}{2})\,\sigma^2}\,exp\left(-\frac{\gamma^2 + 16\,A\,\frac{N_{SFD}}{2})^2}{32\,(\frac{N_{SFD}}{2})\,\sigma^2}\right)\,I_0\left(\frac{A\,\gamma}{\sigma^2}\right) \tag{5.26}$$

Similarly, taking the derivative of P_{fa} w.r.t γ from (5.24) we get the PDF of the second maximum i.e. maximum of side-peaks.

$$p_{second\,max}(\gamma) = \prod_{k=1}^{N_{sym}-N_{SFD}} \left(1 - Q_1\left(\frac{4\,A\,y_k}{\sqrt{\frac{N_{SFD}}{2}}\sigma}, \frac{\gamma}{4\sqrt{\frac{N_{SFD}}{2}}\sigma}\right)\right) \sum_{i=1}^{N_{sym}-N_{SFD}} \left[\frac{p_i(\gamma)}{\left(1 - Q_1\left(\frac{4\,A\,y_i}{\sqrt{\frac{N_{SFD}}{2}}\sigma}, \frac{\gamma}{4\sqrt{\frac{N_{SFD}}{2}}\sigma}\right)\right)}\right] \quad (5.27)$$

where

$$p_i(\gamma) = \frac{\gamma}{16\,(\frac{N_{SFD}}{2})\sigma^2}\, exp\left(-\frac{\gamma^2 + (16\,A\,y_i)^2}{32\,(\frac{N_{SFD}}{2})\sigma^2}\right) I_0\left(\frac{4\,A\,y_i\,\gamma}{(\frac{N_{SFD}}{2})\sigma^2}\right) \quad (Rician\ PDF) \quad (5.28)$$

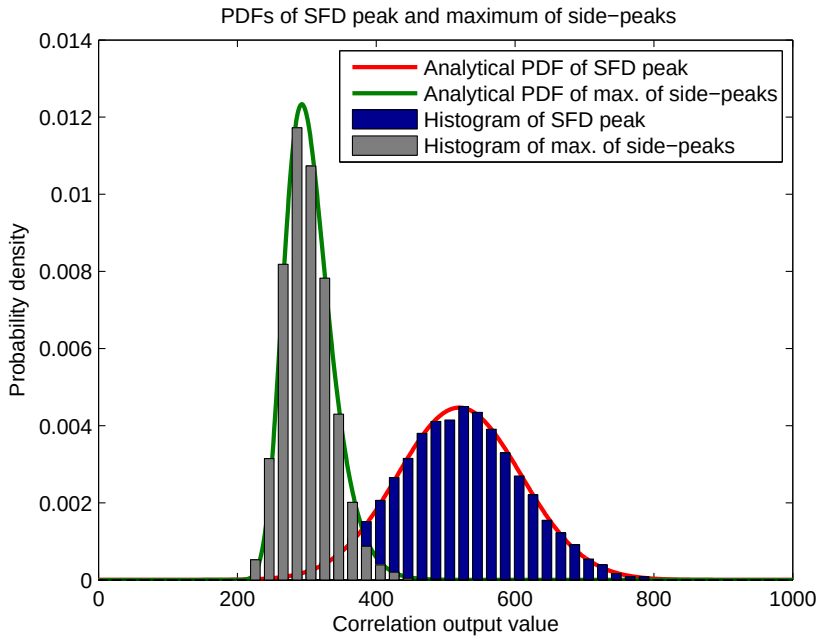

Figure 5.7: PDFs of SFD peak and maximum of side-peaks during coherent detection at -15 dB received SNR per pulse, amplitude A=1

The receiver SFD detection operation was simulated using MATLAB for varying SNR values. By performing monte-carlo simulations, the maximum and second maximum values of the SFD correlation outputs were collected and histograms were plotted. Figure 5.7 shows the histograms obtained from monte-carlo simulations using a SFD sequence of length 64 at -15 dB SNR per pulse. It can be observed that the histograms fit nicely with the analytical PDFs derived for the peak and the maximum of side-peaks.

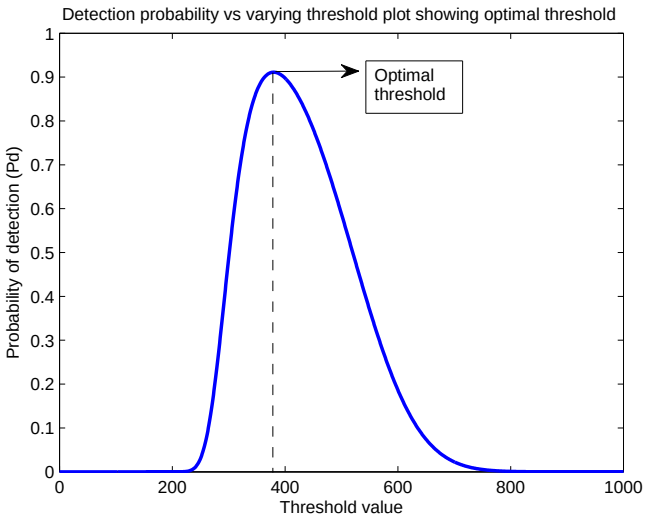

Figure 5.8: Sweeping through threshold (γ) to choose optimal threshold that maximizes P_d at -15 dB SNR per pulse, amplitude A=1

Figure 5.8 shows the plots of the detection probability versus varying threshold value. The threshold value at which the detection probability is maximum is the optimum threshold.

5.4 Non-coherent case

In the non-coherent case, the phase information of the chips sequence (samples) is discarded and the magnitude of the samples is combined.

5.4.1 Symbol Correlation

In the non-coherent case the magnitude of the samples is used for symbol correlation. The distribution of the received samples denoted as $Noisychips$ is Complex Gaussian. After taking the magnitude, the distribution of the samples becomes Rician or Rayleigh depending on whether the mean amplitude of the samples are non-zero or zero i.e. $|a_i| = A$ or 0.

If $a_i = +A, -A$,

$$abs(Noisychips) \sim Rice\left(|a_i|, \sigma\right) \tag{5.29}$$

where $Rice(\nu, \sigma^{'})$ denotes a Rician distributed variable with parameters ν and $\sigma^{'}$.
If $a_i = 0$,

$$abs(Noisychips) \sim Rayleigh\left(\sigma\right) \tag{5.30}$$

Let U_i, the modified preamble code for symbol correlation in non-coherent case.

$U_i = 2|C_i| - 1$ (For zero mean symbol detection)

Let N_{sym} denote the total number of symbols used for the analysis. Each symbol consists of C_{len} samples. Let $SymbolChips$ denote one symbol of length C_{len} from $NoisyChips$. In order to obtain the symbols, $SymbolChips$ is correlated with the known U_i sequence.

$$NcohSym =< Abs(SymbolChips), U_i > \tag{5.31}$$

where $NcohSym$ denotes the symbol obtained by non-coherent combination. The distribution of the noncoherent symbols is given as,

$$NcohSym \sim \sum_{i=1}^{C_{len}} u_i \, Rice\left(|a_i|, \sigma\right) \tag{5.32}$$

The mean of the non-zero samples i.e. Rician variables is given by (see appendix A.3 for expressions),

$$\mu_{rice} = \sigma \sqrt{\frac{\pi}{2}} \, L_{1/2}\left(-\frac{A^2}{2\sigma^2}\right) \tag{5.33}$$

The variance is given by,

$$\sigma^2_{rice} = 2\sigma^2 + A^2 - \mu^2_{rice} \tag{5.34}$$

For Rayleigh variables (zero samples) the mean and variance are given by,

$$\mu_{rayleigh} = \sigma \sqrt{\frac{\pi}{2}} \tag{5.35}$$

$$\sigma^2_{rayleigh} = \frac{(4-\pi)}{2}\sigma^2 \tag{5.36}$$

The U_i sequence consists of sixteen '1's and fifteen '-1's. Thus, $NcohSym$ is obtained as the sum of 16 Rician variables (corresponding to '+1' or '-1' in the C_i code) minus sum of 15 Rayleigh variables (corresponding to '0's in C_i).

$$Ncohsym \sim \sum_{i=1}^{16} Rice\left(A, \sigma\right) - \sum_{i=1}^{15} Rayleigh\left(\sigma\right) \tag{5.37}$$

$$E(Ncohsym) = 16\,\mu_{rice} - 15\,\mu_{rayleigh} \tag{5.38}$$

$$Var(Ncohsym) = 16\,\sigma^2_{rice} + 15\,\sigma^2_{rayleigh} \tag{5.39}$$

The same applies to SFD's non-zero symbols i.e. -1, +1, since taking the absolute value results in '1'.

The '0' symbols of SFD have a normal distribution after adding noise and the distribution of the envelope is therefore Rayleigh. Hence, for zero terms of SFD

$$NcohSym \sim \sum_{i=1}^{16} Rayleigh\,(\sigma) - \sum_{i=1}^{15} Rayleigh\,(\sigma) \tag{5.40}$$

The mean and variance of the '0' symbols are given by,

$$E(NcohSym) = 16\,\mu_{rayleigh} - 15\,\mu_{rayleigh} = \mu_{rayleigh} \tag{5.41}$$

$$Var(Ncohsym) = 16\,\sigma^2_{rayleigh} + 15\,\sigma^2_{rayleigh} = 31\,\sigma^2_{rayleigh} \tag{5.42}$$

5.4.2 SFD correlation

For detecting the SFD, the incoming non-coherent symbols are correlated with the template sequence. The SHR preamble sequence consists of SYNC and SFD symbols corrupted by noise. Let the SFD terms be denoted by b_i. Let the template be denoted by $SFDm$. The terms of $SFDm$ denoted by d_i are given by,

$$d_i = 2\,|b_i| - 1 \tag{5.43}$$

i.e '+1' and '-1' become 1 and '0' becomes -1. This is done to preserve the correlation properties of the SFD sequence. If instead of $SFDm$, the absolute value of the SFD sequence i.e. $|SFD|$ is used for SFD correlation, the correlation output would be as shown in Figure 5.9. Clearly the peak cannot be isolated since the output of the correlation with SYNC portion also has the same amplitude as the SFD correlation peak.

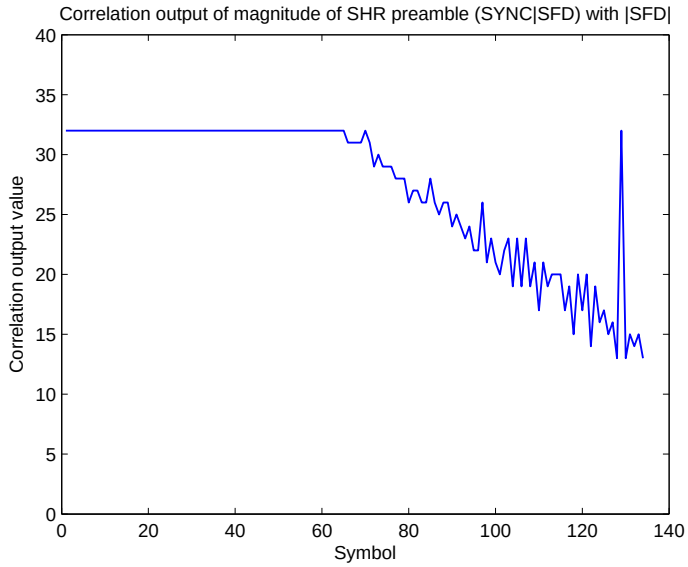

Figure 5.9: Correlation of absolute value of preamble symbols with absolute value of SFD

Let the output of SFD correlation be denoted by Sn.It is obtained as the result of correlating the SFDm template with the received SHR preamble symbols as shown in Figure 5.10. Thus, $Sn(1)$ gives the result of correlation of symbols 1 to N_{SFD} with the $SFDm$ template, $Sn(2)$ gives the result of correlation of symbols 2 to N_{SFD}+1 and so on. Since there are N_{sym} symbols, the number of correlation outputs is $N_{sym} - N_{SFD} + 1$.

$$Block(n) = NcohSym(n), NcohSym(n+1)...NcohSym(n+N_{SFD}-1) \tag{5.44}$$

where 1≤ n ≤ N_{sym}.

$$Sn(n) =< Block(n), SFDm > \tag{5.45}$$

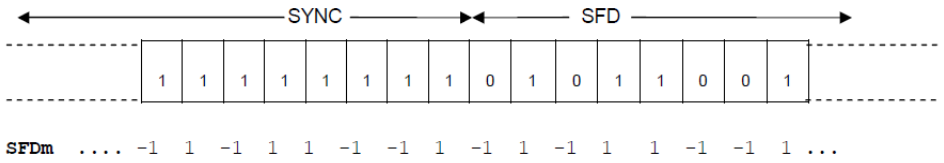

Figure 5.10: SFD correlation of SHR preamble with $SFDm$ in non-coherent case

The $SFDm$ is constructed such that there are equal number of '+1's and '-1's i.e. $\sum d_i = 0$. Figure 5.11 shows the cross correlation of the magnitude of SHR preamble symbols with $SFDm$. The result of the correlation depends on which portion of the SHR preamble is taken, i.e. SYNC, SYNC+SFD or only SFD. In the following, they are analysed separately.

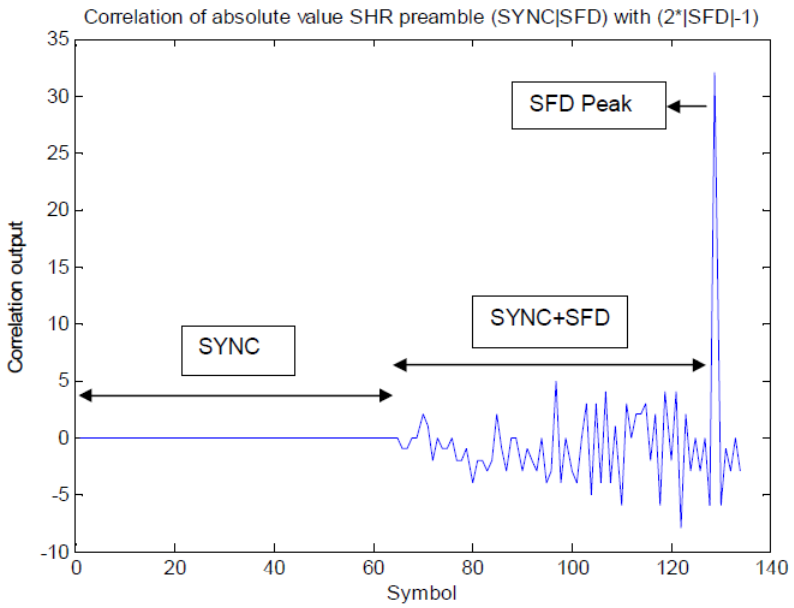

Figure 5.11: SFD correlation output (y) in non-coherent case

5.4.2.1 SYNC portion

The SYNC portion of the SHR preamble consists of a repetition of the S_i symbols. So despreading gives a constant value for all symbols. Since the template sequence has equal number of '+1's and '-1's, adding all the symbols gives zero. In the presence of AWGN , using (5.37), the correlation output has a distribution given by

$$Sn(k) = \sum_{j=1}^{\frac{N_{SFD}}{2}} a_j - \sum_{j=1}^{\frac{N_{SFD}}{2}} b_j \tag{5.46}$$

where $k \in$(SYNC), a_j and b_j are the outputs of non-coherent symbol correlation (i.e. $NcohSym$), having a distribution as given in (5.37).

Using central limit theorem (CLT) [12], the weighted sum of Rayleigh/Rician variables can be approximated as a Gaussian distribution if the number of variables is large. Obtaining Sn involves combining $16\,N_{SFD}$ Rice distributed variables and $15\,N_{SFD}$ Rayleigh variables, where $N_{SFD} = 8$ *or* 64. As the number is large enough, the distribution of the combination of the Rician and Rayleigh variables can be approximated as a Gaussian distribution with mean and variance equal to weighted sum of the means and weighted sum of the variances respectively of the Rician/Rayleigh distributed samples.

Using equation 5.38 the mean of the resulting distribution is given by,

$$E[Sn(k)] = \left(\frac{N_{SFD}}{2}\right)(16\,\mu_{rice} - 15\,\mu_{rayleigh}) - \left(\frac{N_{SFD}}{2}\right)(16\,\mu_{rice} - 15\,\mu_{rayleigh}) = 0 \tag{5.47}$$

The variance is obtained using equation 5.39.

$$Var[Sn(k)] = N_{SFD}(16\,\sigma^2_{rice} + 15\,\sigma^2_{rayleigh}) \tag{5.48}$$

The approximate distribution of the correlation output of this portion is thus,

$$Sn(k) \sim N(0, N_{SFD}\,(16\,\sigma^2_{rice} + 15\,\sigma^2_{rayleigh})) \tag{5.49}$$

5.4.2.2 SYNC+SFD portion

In this case the non-coherent symbols from the tail of SYNC and the initial part of the SFD are correlated with the template sequence. Let $y(i)$ denote the cross correlation output of the i_{th} block which starts at symbol index i(Figure 5.11). Since the magnitude of the symbols is used, the distribution of the '0' symbols in the preamble (SFD) has a non-zero mean (Equation 5.40). So there is a contribution to the result from the zero-symbols as well.

Let $u(i)$ and $v(i)$ denote the arrays of indexes of the non-zero symbols and zero-symbols respectively in the ith block. Let $z(i)$ denote the sum of the terms in $SFDm$ corresponding to the zero-indexes of the SYNC+SFD block starting at the ith symbol position.

In the presence of noise, the correlation output has a distribution given by,

$$Sn(i) \sim \sum_{j=1}^{len(u(i))} (NcohSym(u(i,j)))\, SFDm(u(i,j)) + \sum_{k=1}^{len(v(i))} (NcohSym(v(i,k)))\, SFDm(v(i,k)) \quad (5.50)$$

where $i \in (SYNC + SFD)$.

Using CLT, the distribution of the combination of the Rician and Rayleigh variables can be approximated as a Gaussian distribution with mean and variance equal to weighted sum of the means and sum of the variances of the Rician/Rayleigh distributed samples respectively.

Using equations 5.38 and 5.41, the mean is given by,

$$E[Sn(i)] = y(i)\,(16\,\mu_{rice} - 15\,\mu_{rayleigh}) + z(i)\,\mu_{rayleigh} \quad (5.51)$$

The variance is obtained from equations 5.39 and 5.42,

$$Var[Sn(i)] = len(u(i))\,(16\,\sigma^2_{rice} + 15\,\sigma^2_{rayleigh}) + len(v(i))(31\,\sigma^2_{rayleigh}) \quad (5.52)$$

The approximate distribution of the ith correlation output of this portion is thus given as,

$$Sn(i) \sim N\,(16\,y(i)\,\mu_{rice} - (15\,y(i) - z(i))\,\mu_{rayleigh}, \; 16\,len(u(i))\,\sigma^2_{rice} + (15\,len(u(i)) + 31\,len(v(i)))\sigma^2_{rayleigh}\,) \quad (5.53)$$

5.4.2.3 SFD correlation peak

In this case the non-coherent SFD symbols are correlated with $SFDm$ giving the correlation peak. In the presence of noise, the correlation output is given by,

$$Sn(peak) = \sum_{i=1}^{\frac{N_{SFD}}{2}} Ncohsym(i) - \sum_{j=1}^{\frac{N_{SFD}}{2}} Ncohsym(j) \quad (5.54)$$

where $Ncohsym$ denotes the received symbols in the non-coherent case; i and j denote the indexes of the non-zero SFD symbols and the zero SFD symbols respectively.

The distribution of the non-zero symbols is as given in (5.37) and the zero-symbols are distributed as in (5.37).The distribution of the combination of the Rician and Rayleigh variables can be approximated as a Gaussian distribution with mean and variance equal to weighted sum of the means and sum of the variances of the Rician/Rayleigh distributed samples respectively.

The mean and variance are given by,

$$E[Sn(peak)] = \left(\frac{N_{SFD}}{2}\right)(16\,\mu_{rice} - 15\,\mu_{rayleigh}) - \left(\frac{N_{SFD}}{2}\right)\mu_{rayleigh} \quad (5.55)$$

$$Var[Sn(peak)] = \left(\frac{N_{SFD}}{2}\right)(16\,\sigma^2_{rice} + 15\,\sigma^2_{rayleigh}) + \left(\frac{N_{SFD}}{2}\right) 31\,\sigma^2_{rayleigh} \quad (5.56)$$

The approximate distribution of the correlation peak is thus given as,

$$Sn(peak) \sim N(N_{SFD}\,(8\,\mu_{rice} - 8\,\mu_{rayleigh}), N_{SFD}\,(8\,\sigma^2_{rice} + 23\,\sigma^2_{rayleigh})) \quad (5.57)$$

5.4.3 Evaluation of Threshold

The distributions of the SFD peak and the cross-correlation side peaks in the presence of AWGN in the on-coherent case were derived. Similar to the coherent case, the SFD detection threshold for non-coherent case is also set to the value which maximizes the detection probability.

$$\begin{aligned} P_d &= (1 - P_{fa})\,(1 - P_{miss}) \\ &= (1 - Prob(falsepeaks > threshold))\,(1 - Prob(SFDpeak < threshold)) \end{aligned} \quad (5.58)$$

The probability of false alarm can be expressed as one minus the probability that all the side-peaks are less than the threshold.

$$P_{fa} = 1 - \prod_{i=1}^{N_{sym}-N_{SFD}} P(Sn(i) < threshold) \quad (5.59)$$

The term in the product is given by the CDF of Sn. Since the correlation outputs in the non-coherent case have a gaussian distribution, the cumulative distribution function (CDF) given by the Gaussian Q-function.

The false alarm probability is given by,

$$P_{fa} = 1 - \prod_{i=1}^{N_{sym}-N_{SFD}} \left(1 - Q\left(\frac{\gamma - \mu_i}{\sigma_i}\right)\right) \quad (5.60)$$

where γ denotes the threshold,μ_i and σ_i denote the mean and standard deviation of the corresponding side-peak ($Sn(i)$).

The missed detection probability is the probability of the SFD peak being less than the threshold, which is given by its CDF. Since the distribution of the SFD peak is gaussian, the CDF is given by the gaussian-Q function.

$$P_{miss} = 1 - Q\left(\frac{\gamma - \mu_{peak}}{\sigma_{peak}}\right) \quad (5.61)$$

where γ denotes the threshold, μ_{peak} and σ_{peak} denote the mean and standard deviation of the SFD correlation peak ($Sn(N_{sym} - N_{SFD} + 1)$) (see (eq:SFD peak noncoh dist)).

Combining both, the detection probability is given by,

$$P_d(\gamma) = \left(\prod_{i=1}^{N_{sym}-N_{SFD}} \left(1 - Q\left(\frac{\gamma - \mu_i}{\sigma_i}\right)\right) \right) \left(Q\left(\frac{\gamma - \mu_{peak}}{\sigma_{peak}}\right) \right) \tag{5.62}$$

The threshold γ is chosen such that it maximizes P_d.
Taking the derivative of P_{miss} w.r.t γ from (5.23), we get the PDF of the SFD peak.

$$p_{peak}(\gamma) = \frac{1}{\sqrt{2\pi}\sigma_{peak}} exp\left(-\frac{(\gamma - \mu_{peak})^2}{2\,\sigma_{peak}^2}\right) \tag{5.63}$$

Similarly, taking the derivative of P_{fa} w.r.t γ from (5.24) we get the PDF of the second peak which is maximum of $N_{sym} - N_{SFD}$ side-peaks.

$$p_{second\,max}(\gamma) = \prod_{k=1}^{N_{sym}-N_{SFD}} \left(1 - Q\left(\frac{\gamma - \mu_k}{\sigma_k}\right)\right) \sum_{i=1}^{N_{sym}-N_{SFD}} \left[\frac{\frac{1}{\sqrt{2\pi}\sigma_i} exp\left(-\frac{(\gamma-\mu_i)^2}{2\sigma_i^2}\right)}{\left(1 - Q\left(\frac{\gamma-\mu_i}{\sigma_i}\right)\right)} \right] \tag{5.64}$$

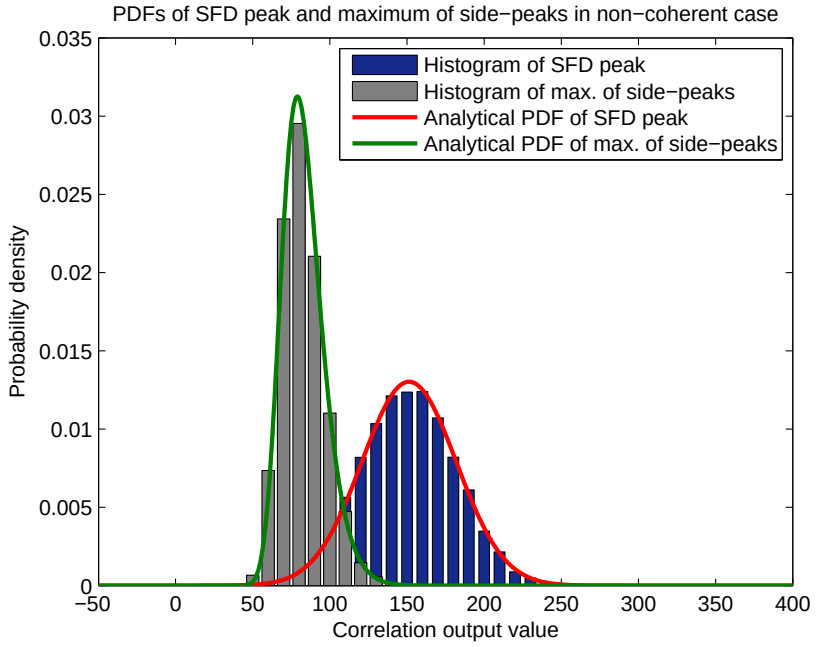

Figure 5.12: PDFs of SFD peak and maximum of side-peaks during non-coherent detection at -3 dB received SNR per pulse, amplitude A=1

Similar to the coherent case, by performing monte-carlo simulations, the maximum and second maximum values of the SFD correlation outputs were collected and histograms were plotted. Figure 5.12 shows the histograms obtained from monte-carlo

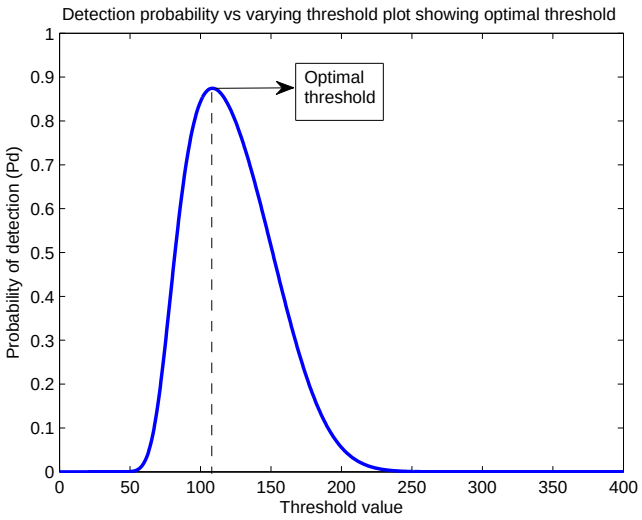

Figure 5.13: Sweeping through threshold (γ) to choose optimal threshold that maximizes P_d at -3 dB SNR per pulse, taking A=1

simulations using a SFD sequence of length 64 at -3 dB SNR per pulse. It can be observed that the histograms fit nicely with the analytical PDFs derived for the peak and the maximum of side-peaks. Figure 5.13 shows the plots of the detection probability versus varying threshold value. It can be seen that the curve has a single maxima for a given SNR. The threshold value at which the detection probability is maximum is the optimum threshold.

5.5 Results

The optimal thresholds for SFD detection are obtained using the probability distributions derived for the correlation outputs in the coherent and non-coherent cases. The threshold is chosen such that it maximizes the detection probability for a given SNR. Figures 5.14 and 5.15 show the plot of threshold versus received SNR per pulse. It can be observed that the threshold is high at lower SNR and decreases gradually with increasing SNR. This is because at low SNR the false alarm probability is relatively higher thus requiring the threshold to be high enough.

Figure 5.16 shows the detection probabilities in both the coherent and non-coherent cases. Clearly the coherent case gives a much better detection performance compared to the non-coherent case. For the length 31 C_i sequence and length 64 SFD sequence considered, the coherent case provides a gain of 12 dB for the same detection performance (around 95% detection probability).

It can also be observed from the plot that using the analytical threshold gives a better performance compared to the current implementation at lower SNR. At 95% detection probabilities the curves are very close. But, using the analytical threshold avoids the complexity involved in collecting statistics from large number of frames for computing a suitable threshold. Instead a lookup table which provides the optimal

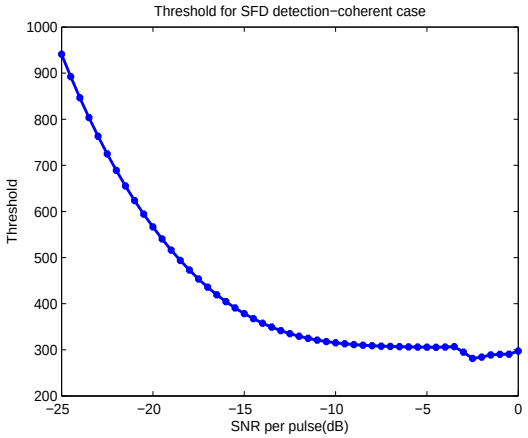

Figure 5.14: SFD detection threshold vs SNR in Coherent case, for amplitude A=1

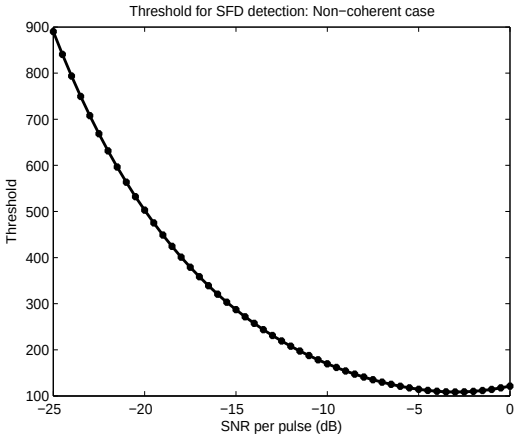

Figure 5.15: SFD detection threshold vs SNR in Non-coherent case, for amplitude A=1

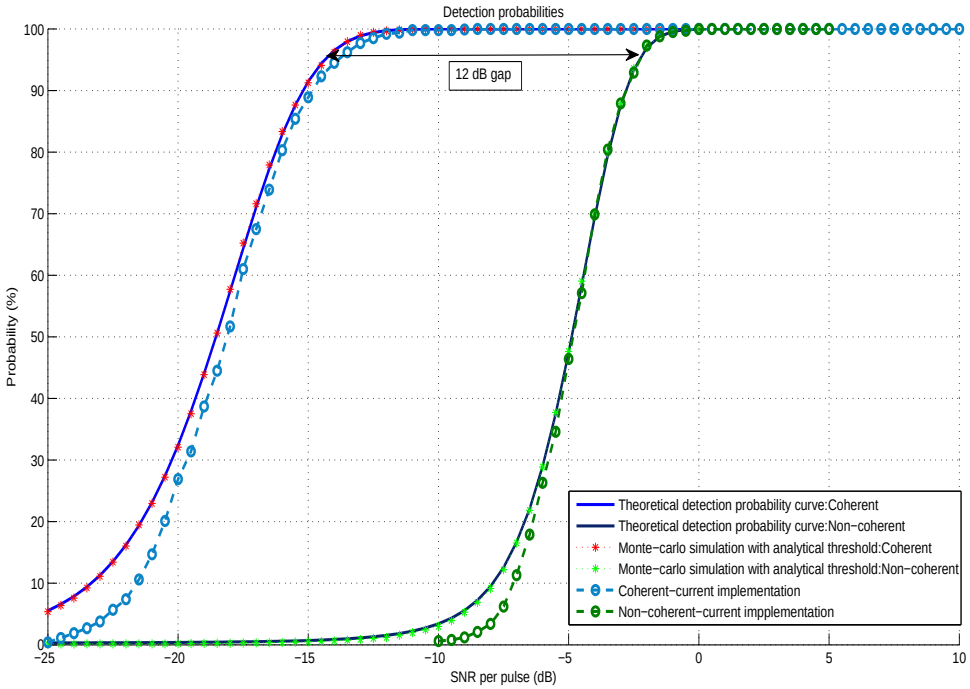

Figure 5.16: SFD detection probability curves: Coherent and Non-coherent

threshold for the given SNR can be used to set the threshold.

5.6 Summary

SFD detection for both coherent and non-coherent cases have been analysed and optimal thresholds for detection have been derived. The optimal threshold is a function of the the received pulse amplitude and noise variance. This information can be obtained from the preamble detection step. Coherent detection gives a much better detection performance compared to non-coherent case. However coherent detection is harder to achieve in the hardware due to its stringent timing requirements. Compared to the current implementation, this method of threshold setting is energy efficient as large number of frames need not be wasted; the thresholds can be directly obtained from a look-up table.

6 Conclusions

6.1 Main contributions and results

This thesis work focused on measurement and analysis of the IR-UWB system. The analysis resulted in a method to optimize the system receiver performance. The main contributions are:

1. **Transmitter measurements**

   Measurements of the transmit output power, spectrum, bandwidth, pulse shape and DC power consumption were performed on IR-UWB transmitter board. It was shown that:

   - The transmitter output spectrum fits almost within the transmit spectrum mask and the channel bandwidth is larger than 500 MHz, as required for a UWB signal.
   - The peak voltage calculated using the peak power measurement using a spectrum analyzer matches with the peak voltage measured on the oscilloscope.
   - From the DC power consumption measurements it is observed that DC power consumption in duty-cycled mode is considerably lower (factor of 45) than in the continuous case.

2. **Method to estimate the received signal to noise ratio (SNR)**

   A method to estimate the signal-to-noise ratio per pulse (SNR) in the preamble detection stage was proposed.

   - The number of frames required for the estimation was analyzed.
   - The SNR estimate is useful in setting threshold for SFD detection.

3. **Threshold for Start of frame delimiter (SFD) detection**

   A theoretical analysis of the SFD detection step of the digital baseband receiver was done for coherent and non-coherent detection. Probability distributions of the SFD correlation output were derived assuming Gaussian channel. Optimal thresholds maximising the detection probabilities were computed. The detection performance was verified by simulations.

   - The threshold is a function of the pulse amplitude and noise variance.
   - The best detection probability that can be achieved, for a given preamble code and SFD sequence, was shown for both coherent and non-coherent cases.
   - Coherent detection gives a 12 dB SNR gain over non-coherent detection for the same detection performance.

- The theoretical approach gives a better performance compared to the current implementation and does not require the receiver to collect large number of frames for setting the threshold.

6.2 Directions for future work

1. In the initial thesis plan, measurement of the IR-UWB receiver was also planned but could not be done as the receiver was not working until the end of the thesis duration. So as an extension of the work the following can be done:
   - Measurement of receiver sensitivity and DC power consumption in the receiver.
   - Verification of SNR estimation in the preamble detection stage using the hardware.
   - Verification of SFD detection performance obtained from theoretical analysis using the hardware.
2. The analysis was carried out only for a additive white gaussian noise (AWGN) channel. It can be extended to other practical channel models. But, this would require the knowledge of the channel at the receiver. The channel information can be obtained in the preamble synchronisation stage of the receiver.
3. A model for the link budget and system power consumption can be made for different modes of operation. Using this model an analysis of the degrees of freedom in the system parameters can be done to choose the optimum set of parameters for different applications.
4. IR-UWB wireless systems are suited to low power short-range applications. However there are other competing narrow-band technologies which use much lower bandwidths and an can support higher data rates. The system design approaches for the narrowband and ultra-wideband cases are quite different. A comparative study of IR-UWB characteristics with other wireless standards can be a possible future work.

Bibliography

[1] Chandrakasan et al.,“ Low-Power Impulse UWB Architectures and Circuits,” Proceedings of the IEEE, vol.97, No.2, February 2009.

[2] FCC, “Revision of part 15 of the commision’s rules regarding ultra-wideband transmission systems,” FCC 02-48, Feb. 2002.

[3] Dieter J.Cichon and Wiener Wiesbeck, “The Heinrich Hertz wireless experiments at Karlsruhe in the view of modern communication,” International Conference on 100 Years of Radio, September 1995

[4] Jorge R.Fernandes; Devid Wentzloff; “Recent Advances in IR-UWB Transceivers: An Overview,” Circuits and Systems (ISCAS), Proceesings of 2010 IEEE International Symposium, pp.3284-3287,June 2010

[5] IEEE 802.15.4a 2007 standard document, section 6.8a UWB PHY specification.

[6] M.Z.Win and R.A. Scholtz, “Impulse radio: How it works,” IEEE Communication Letters, 2(2):36-38, Feb 1998.

[7] Neirynck, D.; Philips, K.; Rousseaux, O.; , “Partially coherent signal combination for impulse radio synchronisation,” Circuits and Systems (ISCAS), Proceedings of 2010 IEEE International Symposium on , vol., no., pp.3292-3295, May 30 2010-June 2 2010

[8] Measurement techniques of ultra-wideband transmissions, ITU-R, Geneva, Switzerland, Recommendation ITU-R SM.1754, 2006.

[9] H.Pflug; J.Romme; K.Philips; H.de Groot; , “Method to estimate impulse-radio ultra-wideband peak power”,IEEE Transactions on Microwave Theory and Techniques, vol.59, No.4, April 2011.

[10] H.Pflug; D.Neirynck; J.Romme; K.Philips; and H.de Groot; “UWB pulse amplitude estimation method for IEEE 802.15.4a,” Proceedings of 2010 IEEE International Conference on Ultra-Wideband , 2010.

[11] H.Pflug, “UWB pulse shaping for IEEE 802.15.4a,” Proceedings of the 38th European Microwave Conference.

[12] John. G. Proakis, “Digital Communications,” McGraw-Hill 2007

[13] Jeremiah Hu; Norman C. Beaulieu;, “Accurate simple closed-form approximations to Rayleigh sum distributions and densities,” IEEE Communications Letters, vol.9, No.2, February 2005.

[14] Li Huang; El Ghouti, N.; Rousseaux, O.; Gyselinckx, B.; , ”Timing Tracking Algorithms for Impulse Radio (IR) Based Ultra Wideband (UWB) Systems,” Wireless Communications, Networking and Mobile Computing, Sept. 2007

Appendix A

A.1 Standard modes

Mode	Preamble				**All**	PHY header				PSDU			
	N_{cpp}	C_{len}	N_{sfd}	Rate Msym/s	N_{hop}	N_{cpb}	N_{cg}	N_{cps}	Rate Msym/s	N_{cpb}	N_{cg}	N_{cps}	Rate Msym/s
1.1	16	31	64	1.006	8	128	1024	4096	0.122	128	1024	4096	0.122
1.2	16	31	8	1.006	8	16	128	512	0.975	16	128	512	0.975
1.3	16	31	8	1.006	8	16	128	512	0.975	2	16	64	7.800
1.4	16	31	8	1.006	8	16	128	512	0.975	1	8	32	15.60
2.1	64	31	64	0.252	32	32	1024	4096	0.122	32	1024	4096	0.122
2.2	64	31	8	0.252	32	4	128	512	0.975	4	1287	5127	0.975
2.3	64	31	8	0.252	32	4	128	512	0.975	2	64	256	1.950
2.4	64	31	8	0.252	32	4	128	512	0.975	1	32	128	3.900
3.1	4	127	64	0.983	2	512	1024	4096	0.122	512	1024	4096	0.122
3.2	4	127	8	0.983	2	64	128	512	0.975	64	128	512	0.975
3.3	4	127	8	0.983	2	64	128	512	0.975	8	16	64	7.800
3.4	4	127	8	0.983	2	64	128	512	0.975	2	4	16	31.20

Table A.1: Standard modes

Note: The mode numbers are not given in the IEEE standard. They are used only in Holst centre/imec.

A.2 Calculating IR-UWB Signal Power

A.2.1 Average and Peak Signal Power

One of the parameters used is the signal peak amplitude, V_{pk}, as shown in Figure A.1

Using this, the burst power (for a single pulse or burst of pulses) is defined as:

$$P_{burst} = \frac{V_{pk}^2}{(2 * 50)} \quad (W) \tag{A.1}$$

This burst power is the instantaneous power measured during the existence of the burst.

The average power, measured when a power meter is connected to the signal is:

$$P_{avg} = P_{burst} * dc \quad (W) \tag{A.2}$$

where dc is the duty cycle of the signal, equal to 1/(number of burst hopping positions per symbol) $dc = 1/N_{hops}$

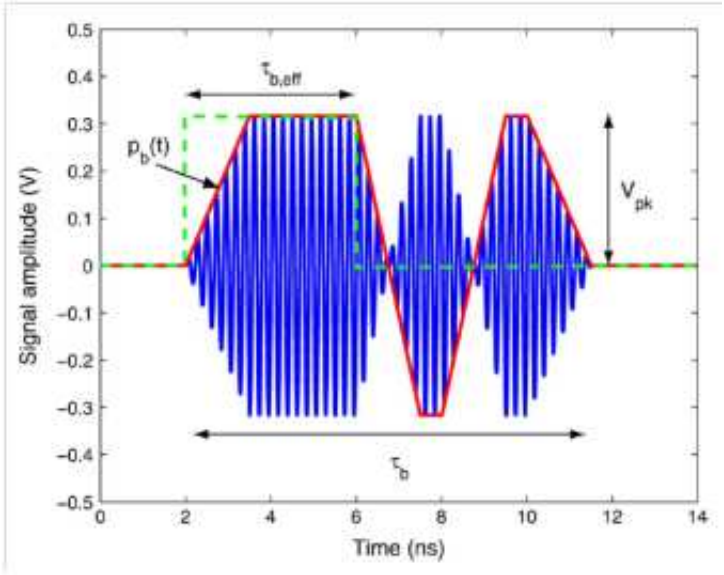

Figure A.1: fig:IEEE 802.15.4a IR-UWB signal example showing V_{pk} being the peak amplitude.

The energy per pulse is calculated as:

$$E_p = P_{burst} * \tau_c \quad (J) \tag{A.3}$$

In which τ_c is the effective pulse width of a single pulse or chip. In the case of this standard:

$$\tau_c = \frac{1}{499.2e6} \quad (s) \tag{A.4}$$

A.2.2 Regulatory Signal Power

The UWB regulatory requirements specify both average and peak power values. These can be calculated from V_{pk} using the following equations:

$$P_{avg,1MHz} = P_{avg} * 1e6/500e6 \quad (W,\ measured\ in\ 1\ MHz) \tag{A.5}$$

where 1e6 is the measurement bandwidth of 1 MHz and 500e6 is the pulse bandwidth of 500 MHz.

Mode	**dc**	α_b
1.2	3.125	0.998
Demo	3.125	1.000
2.2	0.781	0.550

Table A.2: Mode dependent parameter values

$$P_{pk,50MHz} = P_{burst} * \alpha_b^2 \quad (W,\ measured\ in\ 50\ MHz) \tag{A.6}$$

where α_b is the burst desensitisation factor. Table A.2 lists this parameter for some modes.

Signal power	**Equation**	**Unit**
Burst power	$P_{burst} = (V_{pk}^2)/(2 * 50)$	(W)
Average power	$P_{avg} = P_{burst} * dc$	(W)
Pulse energy	$E_p = P_{burst} * \tau_c$	(J)
Regulatory average power	$P_{avg,1MHz} = P_{avg} * 1e6/500e6$	(W) in 1 MHz
Regulatory peak power	$P_{pk,50MHz} = P_{burst} * \alpha_b^2$	(W) in 50 MHz

Table A.3: Summary

A.3 Probability distributions

1. **Gaussian distribution**

   The probability density function of a random variable X having a Gaussian distribution with mean μ and variance σ^2 i.e. $N(\mu, \sigma^2)$, is given by

$$p_X(x) = \frac{1}{\sqrt{2\,\pi\,\sigma^2}}\, exp(-\frac{(x-\mu)^2}{2\,\sigma^2}) \tag{A.7}$$

   The cumulative distribution function is given by,

$$P(X \leq a) = 1 - Q(\frac{a-\mu}{\sigma}) \tag{A.8}$$

   where $Q(.)$ denotes the gaussian Q function.

2. Rician distribution

   The probability density function of a random variable Y having a Rice distribution with parameters ν and σ i.e. $Rice\,(\nu, \sigma)$, is given by,

$$p_Y(y) = \frac{y}{\sigma^2}\, exp\left(\frac{-(y^2+\nu^2)}{2\,\sigma^2}\right)\, I_0\left(\frac{\nu\, y}{\sigma^2}\right) \tag{A.9}$$

   the CDF is given by,

$$P(Y \leq a) = Q_1\left(\frac{\nu}{\sigma}, \frac{a}{\sigma}\right) \tag{A.10}$$

   where $Q_1(,)$ denotes the Marcum-Q function.

   The mean of the Rician variable with parameters ν and σ is given by,

$$\mu_{rice} = \sigma\,\sqrt{\frac{\pi}{2}} L_{1/2}(-\frac{\nu^2}{2\sigma}) \tag{A.11}$$

where L_q denotes a Laguerre polynomial. For q=1/2 it equals,

$$L_{1/2}(x) = exp(\frac{x}{2})((1-x)I_0(-\frac{x}{2}) - x\, I_1(\frac{-x}{2})) \tag{A.12}$$

$I_n(x)$ denotes the modified bessel function of nth order.

The variance is given by,

$$\sigma^2_{rice} = 2\sigma^2 + \nu^2 - \mu^2_{rice} \tag{A.13}$$

3. Rayleigh Distribution

   The probability density function of a random variable X having a Rayleigh distribution with parameter σ i.e. $Rayleigh\,(\sigma)$, is given by,

$$p_Z(z) = \frac{z}{\sigma^2}\, exp\left(\frac{-z^2}{2\,\sigma^2}\right) \tag{A.14}$$

   The CDF is given by,

$$P(Z \leq a) = 1 - exp\left(\frac{-a^2}{2\sigma^2}\right) \tag{A.15}$$

   For a Rayleigh variable with parameter $\sigma^{'}$the mean and variance are given by,

$$\mu_{rayleigh} = \sigma^{'}\sqrt{\frac{\pi}{2}} \tag{A.16}$$

$$\sigma^2_{rayleigh} = \frac{(4-\pi)}{2}\sigma^{'2} \tag{A.17}$$